RSC Advances

PAPER

View Article Online
View Journal | View Issue

Cite this: *RSC Adv.*, 2023, **13**, 22122

Design, synthesis, *in silico* studies, and biological evaluation of novel pyrimidine-5-carbonitrile derivatives as potential anti-proliferative agents, VEGFR-2 inhibitors and apoptotic inducers†

Abdulrahman M. Saleh, [ab] Hazem A. Mahdy, *[a] Mohamed Ayman El-Zahabi,[a] Ahmed B. M. Mehany,[b] Mohamed M. Khalifa *[a] and Ibrahim H. Eissa *[a]

A novel series of pyrimidine-5-carbonitrile derivatives bearing benzylidene and hydrazone moieties with different linkers (spacers) were designed and synthesized as possible inhibitors of the vascular endothelial growth factor receptor-2 (VEGFR-2). The newly synthesized compounds were evaluated *in vitro* for their cytotoxic activities against two human cancer cell lines namely colon cancer (HCT-116) and breast cancer (MCF-7) using sorafenib as a standard anticancer drug. Compounds **9d**, **11e**, **12b**, and **12d** showed higher cytotoxic activities than sorafenib with IC_{50} values ranging from 1.14 to 10.33 μM. In particular, compound **11e** exhibited excellent activities against HCT-116 and MCF-7 with IC_{50} values of 1.14 and 1.54 μM, respectively. Moreover, compound **11e** exhibited about 47.32-fold cytotoxic activity against normal human fibroblast (WI-38) cells, lower than the cytotoxicity against the cancer cells. Compounds **11e** and **12b** were the most potent VEGFR-2 inhibitors with IC_{50} values of 0.61 and 0.53 μM, respectively, compared to sorafenib. Bedsides, compound **11e** arrested the HCT-116 cell growth at S and sub-G1 phases, induced a significant increase in the apoptotic cells, and caused remarkable decrease in the levels of TNF-α, IL-6, and caspase-3. Finally, the binding patterns of the target derivatives were investigated through the docking study against the proposed molecular target (VEGFR-2, PDB ID 1YWN). The results of molecular docking studies showed similar binding modes to sorafenib against VEGFR-2. In addition, molecular dynamic simulations revealed the stability of compound **11e** in the active site for 100 ns.

Received 21st June 2023
Accepted 11th July 2023

DOI: 10.1039/d3ra04182d

rsc.li/rsc-advances

1. Introduction

Cancer, a disease characterized by uncontrollable cell growth, is still one of the most serious diseases to threaten human life.[1] Although there are wide advances dealing with its biochemistry and trying to understand its progression, the complete cure of cancer has not been achieved yet.[2–4] The increased incidence of cancer cases returns primarily to the resistance of the cancer cells to the known medications, the reason that opens the door to research to either find new targets or to construct new chemical scaffolds to act on the previously identified targets.

Vascular Endothelial Growth Factor (VEGF) has been nominated as one of the most prevalent tumor angiogenesis mediators. VEGF initiates endothelial cell activation and proliferation.[5] However, it promotes vascular permeability in solid tumors.[6] These processes are all mediated *via* stimulation of a specific type of tyrosine kinase receptors, VEGFR-2 receptor.[7] However, VEGF/VEGFR-2 pathway contributes to the progress of numerous cancer types including breast, colon, gastric and lung *via* migration, metastasis and stimulation of angiogenesis.[8] Therefor hindering the VEGF/VEGFR-2 pathway appears crucial in stopping angiogenesis.[9] Accordingly, VEGFR-2 gained an increasing importance in the anti-angiogenic therapy against cancer. Unfortunately, treatment with the currently FDA approved VEGFR-2 inhibitors faced several drawbacks represented in their serious adverse reactions and development of a secondary resistance.[10] There drawbacks motivated the medicinal chemists to continue searching for new small molecules aiming to overcome the adverse effects and minimize resistance.[11–14]

Observing the structure–activity relationship of the FDA approved VEGFR-2 inhibitors revealed that they almost shared four common features namely, (a) a heterocyclic head with minimum one nitrogen atom to occupy the hinge region of the active site, (b) a spacer to occupy gatekeeper region, (c) a hydrogen bonding moiety or a pharmacophore that makes

[a]*Pharmaceutical Medicinal Chemistry & Drug Design Department, Faculty of Pharmacy (Boys), Al-Azhar University, Cairo 11884, Egypt. E-mail: Ibrahimeissa@azhar.edu.eg; Hazem_hady2001@azhar.edu.eg; MohamedKhalifa2321.el@azhar.edu.eg*

[b]*Zoology Department, Faculty of Science (Boys), Al-Azhar University, Cairo 11884, Egypt*

† Electronic supplementary information (ESI) available. See DOI: https://doi.org/10.1039/d3ra04182d

essential H-bonds with the DFG amino acids, and (d) a hydrophobic tail that fills the receptor's allosteric site[15–20] (Fig. 1A). However, Fig. 1B illustrated the role of sorafenib in inhibiting the VEGFR-2-mediated angiogenesis effect.

In light of the abovementioned facts, we were encouraged to build a new scaffold constructed from the four key reported VEGFR-2 inhibitors features. The rationale of our molecular design depended basically on the bioisosteric modification of the well-defined VEGFR-2 inhibitors at their four main parts. However, the 6-aryl-5-cyano-thiouracil moiety was used in the current as a heterocyclic head. The choice of such a moiety was suitable as it contains a pyrimidine core that can fill the large size space of the ATP binding region. Besides, the pyrimidine's nitrogen atoms may serve as H-bond acceptors that may potentiate binding of the designed compounds with the VEGFR-2 receptor. Supporting with the structure of sorafenib **I**, the potent VEGFR-2 inhibitor, we have designed the spacer part of the target members to share the same length of that of sorafenib. The spacer part, hence, consisted of a four-carbon bridge attached to an NH group which are directly linked to heterocyclic head. The length of the designed linker was then convenient to occupy the gate keeper region in VEGFR-2 pocket (Fig. 2).

Two different hydrophilic moieties were selected in the current study to play the role of the compounds' pharmacophore part. The choice of the moieties was based on their ability to act either as H-bond donor or acceptor. Thus, they could bind to the two essential receptor's amino acids, Glu883 and Asp1044. The final position to be modified was the terminal hydrophobic tail. Herein, we fixed the sorafenib phenyl hydrophobic tail with a change in its substitutions as we selected a wide variety of substitutions that enabled us to study the SAR

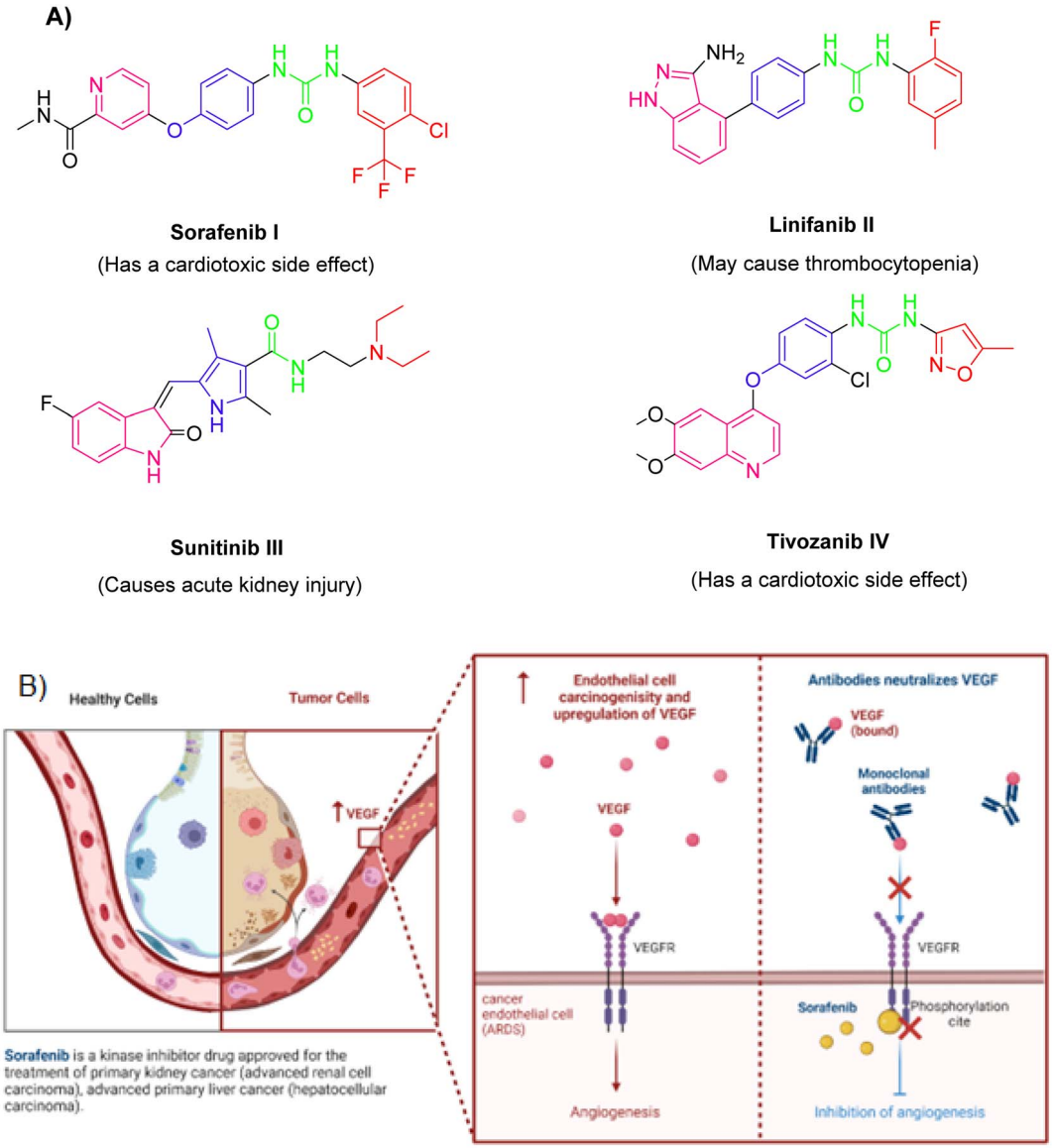

Fig. 1 (A) Some reported VEGFR-2 inhibitors and their necessary four parts. (B) Function of VEGFR-2 and effects of sorafenib.

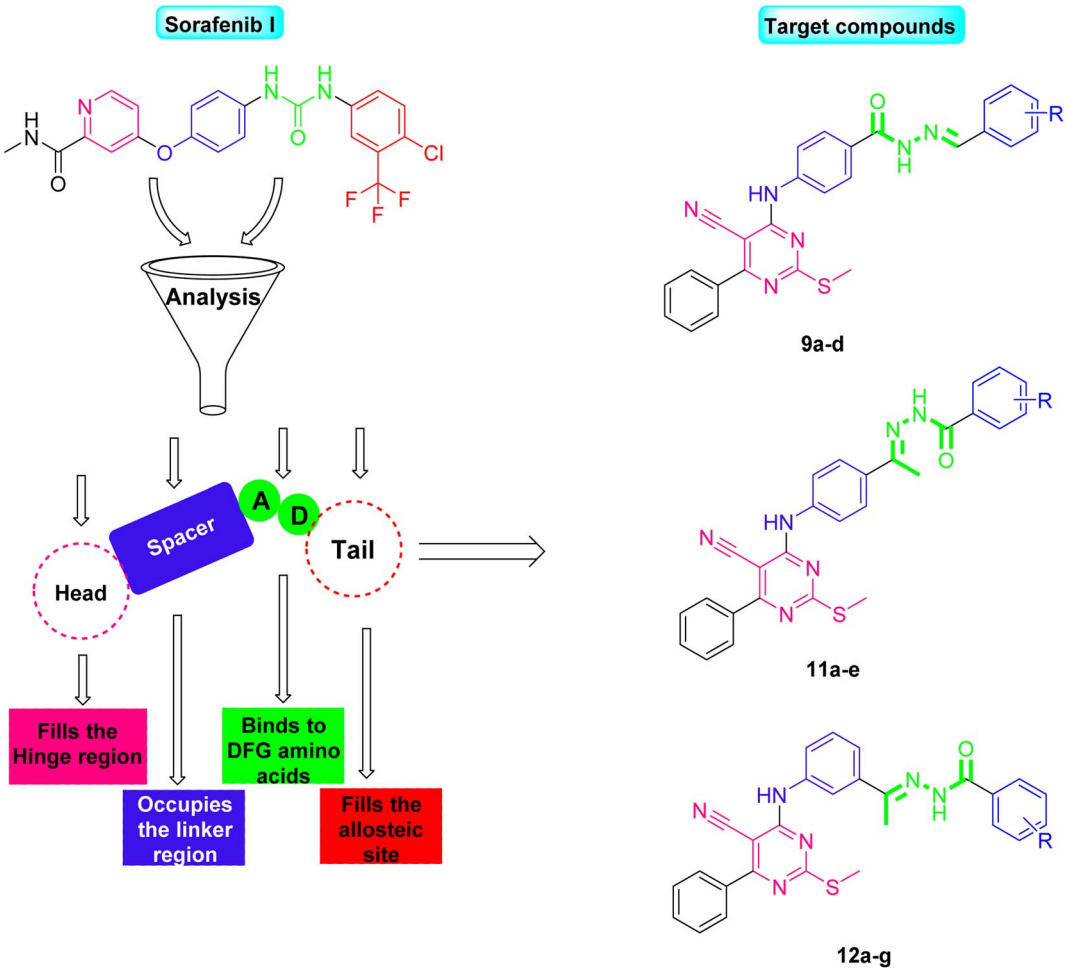

Fig. 2 Rationale of molecular design for synthesis of novel VEGFR-2 inhibitors.

of the designed compounds against VEGFR-2 tyrosine kinase receptor (Fig. 2).

2. Results and discussion

2.1. Chemistry

Chemical reactions for the synthesis of the target derivatives were depicted in Schemes 1–3. First, the starting material 2-mercapto-6-oxo-4-phenyl-1,6-dihydropyrimidine-5-carbonitril **1** was obtained in a good yield by the cyclocondensation of benzaldehyde with ethyl cyanoacetate and thiourea in alkaline media according to the reported method.[21–23] The derivative **1** was subjected to the alkylation with an equivalent amount of methyl iodide in 10% alcoholic KOH to afforded 2-(methylthio)-6-oxo-4-phenyl-1,6-dihydropyrimidine-5-carbonitrile **2**. Thus, refluxing of compound **2** with phosphorus oxychloride afforded the corresponding the key intermediate **3**. The latter **3** was refluxed in *n*-butanol with the commercially available aromatic amines namely, 4-aminobenzoic acid, 4-aminoacetophenone, and 3-aminoacetophenone to yield the corresponding target intermediates **4**, **5**, and **6**, respectively (Scheme 1).

The ^{1}H NMR analyses of such intermediates (**4**, **5**, and **6**) showed three exchangeable signals at δ 10.12, 10.15, and 10.10 ppm corresponding to the NH protons, respectively. Besides, the ^{1}H NMR spectra of **5** and **6** exhibited characteristic singlet signal for $COCH_3$ group resonating at rang of δ 2.53–2.58 ppm.

In order to accomplish the target final compounds, the intermediate **4** was firstly activated by refluxing with thionyl chloride according to the reported method[16] to achieve the acid chloride derivative **7** which was then utilized as freshly prepared without further purification to react with hydrazine hydrate in absolute ethanol to afford acid hydrazide analog **8**. Such reaction was performed using an ice bath to avoid desulfurization which may take place through the attack hydrazine hydrate on the SCH_3 group. The evidences for the formation of the acid hydrazide was verified by spectral data. The IR spectrum displayed strong bands at 3296, 3202 and 1658 cm^{-1} corresponding to NH, NH_2 and C=O groups, respectively. ^{1}H NMR spectrum revealed appearance of a broad singlet signal at δ 4.72 ppm that refers to NH_2 protons and another two singlet signals of two NH groups at δ 9.97 and 9.74 ppm. Then, the hydrazide **8** was allowed to react with appropriate aldehydes at refluxing ethanol temperature in the presence of a catalytic amount of glacial acetic acid to obtain the respective imine compounds or Schiff's bases **9a–d** (Scheme 2).

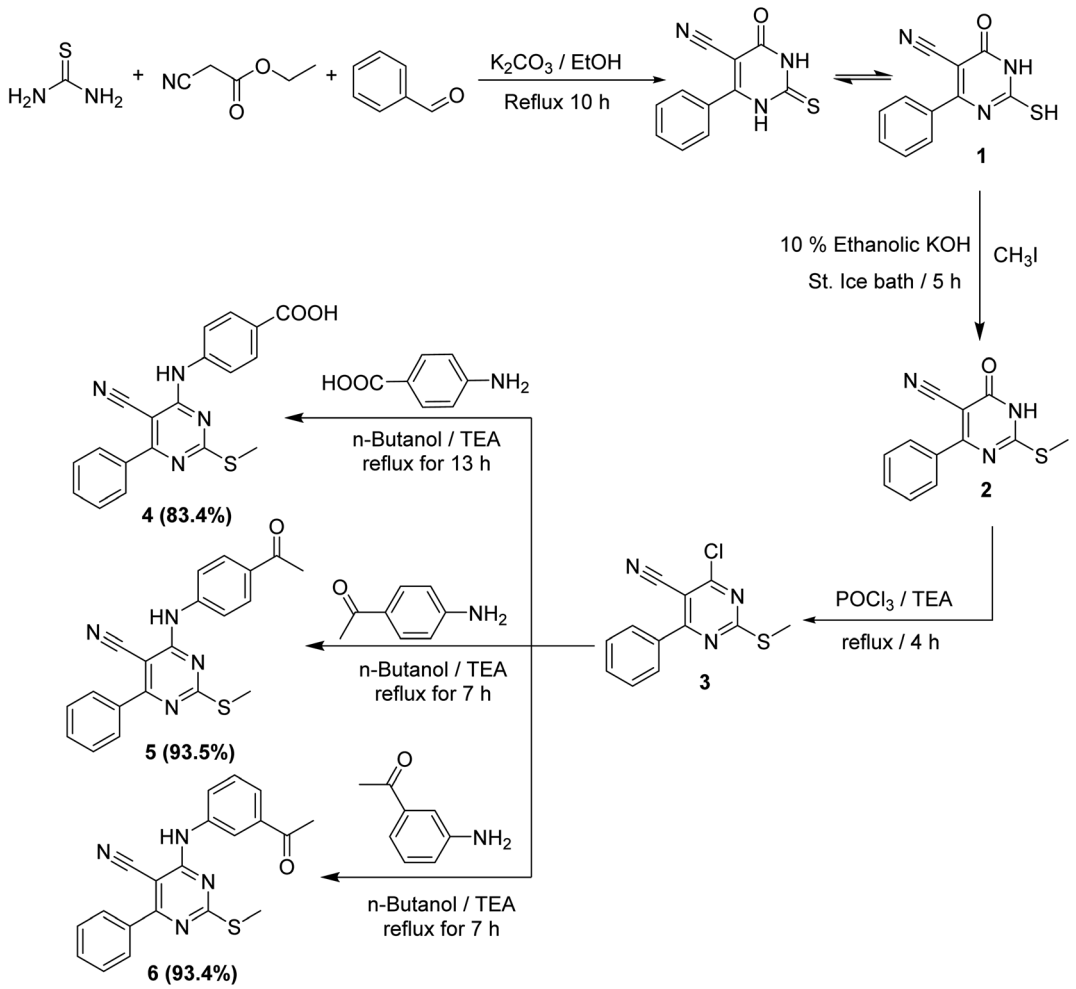

Scheme 1 General procedure for synthesis of intermediate compounds **4**, **5**, and **6**.

IR spectra of these compounds showed the disappearance of NH_2 absorption band of the hydrazide compound **8**. On the other hand, ^{1}H NMR spectra of such compounds displayed a down-field singlet signal at a range of δ 8.84–8.00 ppm that refers to the new benzylidene proton, in addition to an increase in the aromatic protons by five, four or three protons according to the aldehyde used.

Condensation of the keton derivatives **5** and **6** with the appropriate acid hydrazides **10a–g** (obtained according to the reported procedures)[16,23,24] at heating and refluxing temperature in absolute ethanol containing catalytic amount of glacial acetic acid afforded the respective hydrazono compounds **11a–e** and **12a–g**, respectively (Scheme 3).

IR spectra of **11a–e** and **12a–g** series confirmed presence of the carbonyl absorption band at a range of 1666–1637 cm^{-1} and NH bands at a range of 3341–3196 cm^{-1}. On the other hand, the ^{1}H NMR spectra showed up-field singlet signals of the aliphatic SCH_3 and CH_3 protons at δ range of 2.51–2.42 ppm and 2.44–2.20 ppm as well as the presence of NH protons at a δ range of 11.13–9.90 ppm. An important point was noticed regarding a couple of compounds, **11b** and **12b**, as the ^{1}H NMR analyses revealed that they existed as *E*/*Z* isomers. This conclusion was reached through the investigation of signaling patterns of two methyl groups and two NH groups. For compound **11b**, the two isomers appeared as about 60% : 40%. While, for compound **12b**, the two isomers appeared as about 65% : 35%. Complete details for signaling ratio of each signal group were illustrated in ESI (Table S-1 and ^{1}H NMR charts).† Moreover, the ^{13}C NMR spectra of such series showed signals of the two methyl carbons at δ range of 19.20–13.77 ppm.

2.2. Biological evaluation

2.2.1. *In vitro* growth inhibitory activity against HCT-116 and MCF-7 cell lines. The target derivatives were assessed for their *in vitro* anti-proliferative activities of against two overexpressed VEGFR-2 cells; colon cancer (HCT-116), and breast cancer (MCF-7) cell lines *via* MTT assay method.[25–27] Results of the *in vitro* evaluation against HCT-116 and MCF-7 cell lines revealed that these compounds possessed high inhibitory activity towards the two cell lines with IC_{50} ranges of 1.14–32.16 μM. Four out of the thirteen target compounds (**9d**, **11e**, **12b**, **12d**) showed higher cytotoxic activity than the standard sorafenib (IC_{50} = 8.96 and 11.83 μM) with IC_{50} values ranging from 1.14 to 10.33 μM against HCT-116 and MCF-7, respectively. In

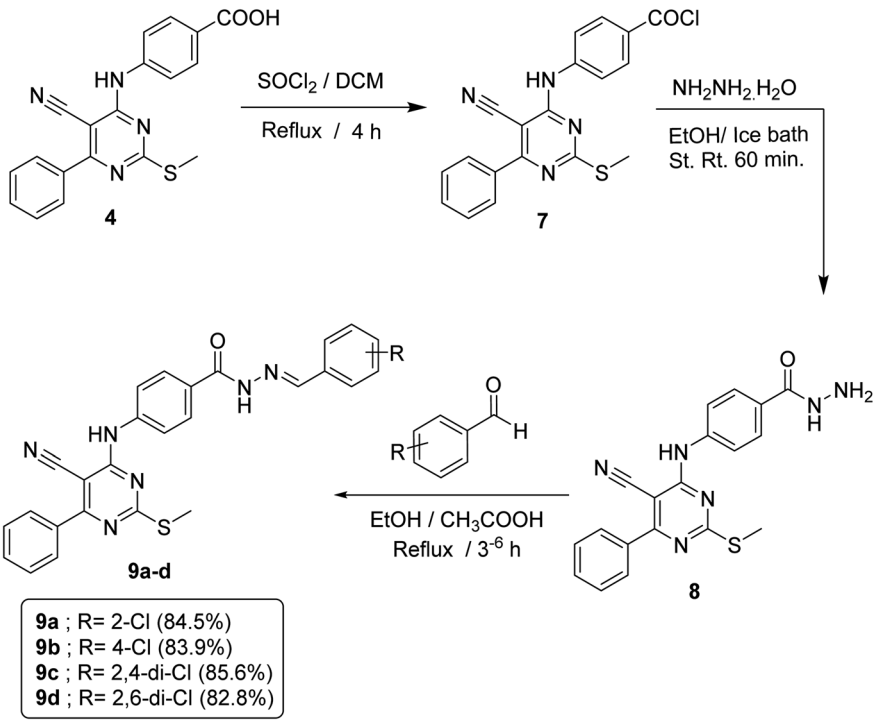

Scheme 2 General procedure for synthesis of target compounds **9a–d**.

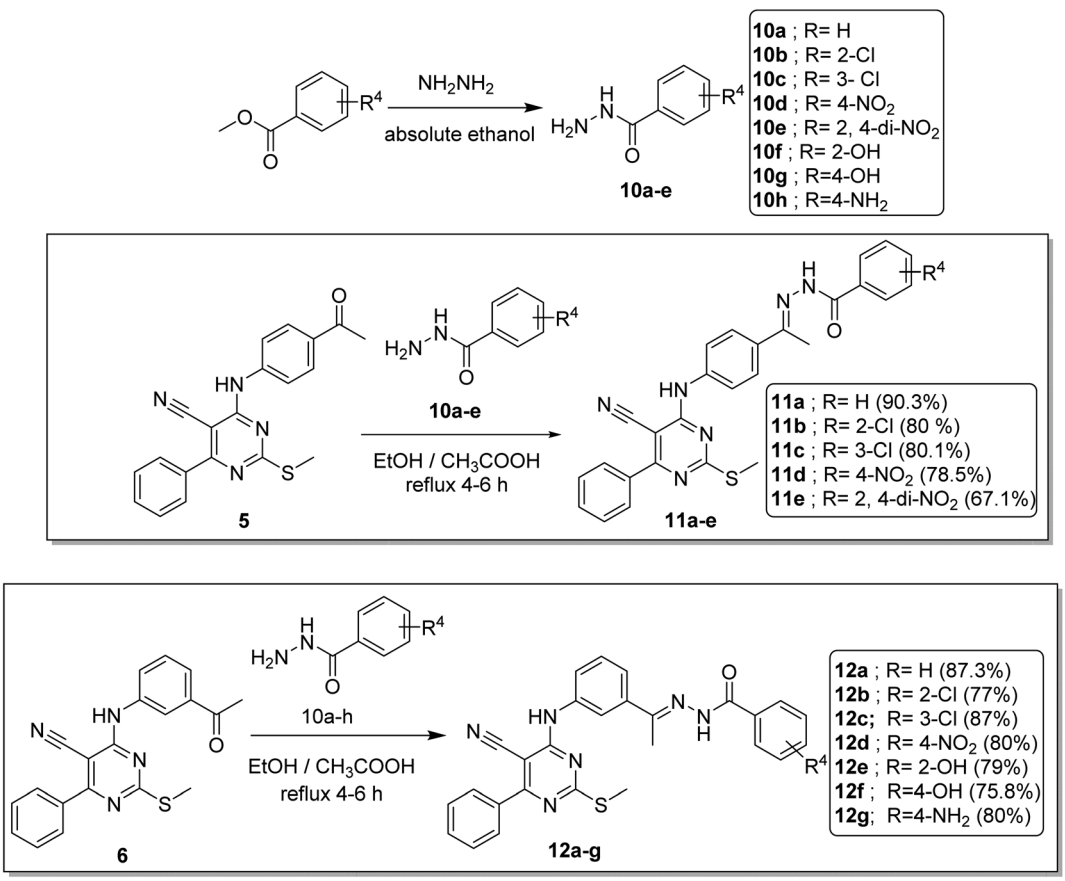

Scheme 3 General procedure for synthesis of target compounds **11a–e** and **12a–g**.

Table 1 *In vitro* anti-proliferative activities of the synthesized compounds against HCT-116 and MCF-7 cell lines their VEGFR-2 inhibitory activities on HCT-116 cell line and cytotoxicity for compound **11e** against normal human lung cells (WI-38)

	In vitro cytotoxicity IC_{50}[a] (μM)			
Comp. no.	HCT 116	MCF-7	WI-38	VEGFR-2[a] (μM)
9a	30.15 ± 0.25	28.66 ± 0.2	NT[b]	NT[b]
9b	12.34 ± 0.09	15.26 ± 0.12	NT[b]	NT[b]
9c	20.62 ± 0.15	26.75 ± 0.24	NT[b]	NT[b]
9d	7.14 ± 0.025	9.85 ± 0.035	NT[b]	2.41 ± 0.16
11a	23.58 ± 0.18	32.16 ± 0.28	NT[b]	NT[b]
11b	10.7 ± 0.05	13.48 ± 0.1	NT[b]	1.55 ± 0.25
11c	10.45 ± 0.05	10.92 ± 0.05	NT[b]	1.38 ± 0.03
11d	13.78 ± 0.11	14.31 ± 0.15	NT[b]	2.32 ± 0.21
11e	1.14 ± 0.01	1.54 ± 0.01	63.41 ± 0.015	0.61 ± 0.01
12a	17.98 ± 0.15	25.18 ± 0.19	NT[b]	NT[b]
12b	8.65 ± 0.05	9.77 ± 0.06	NT[b]	0.53 ± 0.07
12c	9.25 ± 0.07	10.17 ± 0.05	NT[b]	0.74 ± 0.15
12d	7.15 ± 0.06	10.33 ± 0.05	NT[b]	1.61 ± 0.18
12e	19.44 ± 0.14	30.14 ± 0.26	NT[b]	NT[b]
12f	21.36 ± 0.15	26.11 ± 0.18	NT[b]	NT[b]
12g	16.39 ± 0.12	21.72 ± 0.15	NT[b]	NT[b]
Sorafenib	8.96 ± 0.05	11.83 ± 0.07	NT[b]	0.19 ± 0.15

[a] Data are presented as mean ± S. D of the IC_{50} values from two different experiments. [b] NT: not tested.

particular, compound **11e** exhibited excellent activities against HCT-116 and MCF-7 with IC_{50} values of 1.14 and 1.54 μM, respectively. Moreover, four compounds such as **9b**, **11b**, **11c**, **11d**, and **12c** showed remarkable activities against two cell lines with IC_{50} values ranging from 9.25 to 15.26 μM. These results were found to be a little lower than the standard drug. On the other hand, several compounds showed moderate to weak anti-proliferative activities against the tested cell lines.

2.2.2. *In vitro* cytotoxicity against normal human lung cells (WI-38). In order to assess the selectivity of the target compounds against cancer cells over normal ones, the cytotoxicity of the most active compound **11e** was estimated *in vitro* against normal human lung cells (WI-38). The obtained results revealed that, compounds **11e** exhibited cytotoxic IC_{50} value of 63.41 ± 0.015 μM against normal human lung cells. These results indicated that its cytotoxicity against normal cells is about 47.32-fold lower than the cytotoxicity against the cancer cells (Table 1).

2.2.3. *In vitro* VEGFR-2 kinase inhibitory assay. The most active derivatives (**9d**, **11b**, **11c**, **11d**, **11e**, **12b**, **12c**, and **12d**) that exhibited promising anti-proliferative activities were subjected to further investigation for their ability to inhibit VEGFR-2 using sorafenib as a reference VEGFR-2 inhibitor.[28,29] Kinase assay protocol was utilized in this test using Human VEGFR-2 TK ELISA kit. The results of VEGFR-2 inhibitory activity revealed that the compounds showed inhibitory activity with IC_{50} values ranging from 0.53 to 2.41 μM. Compounds **11c**, **11e**, **12b**, and **12c** were the most potent VEGFR-2 inhibitors with IC_{50} values of 1.38 ± 0.03, 0.61 ± 0.01, 0.53 ± 0.07, and 0.74 ± 0.15 μM, respectively, compared with that of sorafenib (IC_{50} = 0.19 ± 0.15 μM). On the other hand, compounds **9d**, **11b**, **11d**, and **12d** showed promising activity towards VEGFR-2 with IC_{50} values of 2.41 ± 0.16, 1.55 ± 0.25, 2.32 ± 0.21, 1.61 ± 0.18 μM, respectively.

2.2.4. Structure–activity relationships (SAR). As outlined in the rationale molecular design, we aimed at studying the SAR of newly synthesized pyrimidine derivatives as potential VEGFR-2 TK inhibitors. Observing the results of different biological tests (*in vitro* anti-proliferative activity, measurement of VEGFR-2 TK activity), we could deduce valuable data about the structure–activity relationships.

• Comparing the cytotoxicity of compounds containing *m*-disubstituted linkers (**12d**, **12b**, **12a**, and **12g**) with their corresponding compounds of the *p*-disubstituted linkers (**11d**, **11b**, and **11a**), respectively, indicated that, the *m*-disubstituted derivatives are more active than the *p*-disubstituted ones (Fig. 3).

With regard to the benzylidene derivatives (containing hydrazone moiety) **9a–d**:

• The p-electron withdrawing substitution derivatives (**9b**) were more active than these with *o*-electron withdrawing ones (**9a**) (Fig. 4).

• Introduction of a chlorine atom at *p*-position exhibited preferable activity than *o*-position. Meanwhile, di-chloro substitution at 2,6-positions (**9d**) showed an activity stronger than the *p*-substituted one, but 2,4-dichloro derivative (**9c**), elicited lower activity than both (Fig. 5).

• Compound **11e** containing di-nitro substitution at 2,4-positions showed the highest cytotoxic activity on the both tested cell lines, moreover, shifting the nitro group from *o*-position showed a sever decreasing in cytotoxicity and VEGFR-2 TK inhibitory activity (Fig. 6).

• Shifting the chloro group from *m*-position (**11c**) to *o*-position (**11b**) showed notable decrease in the cytotoxic activity (Fig. 7).

Regarding to the derivatives **12a–g** containing *m*-disubstituted linkers, observation of the cytotoxic activity revealed that:

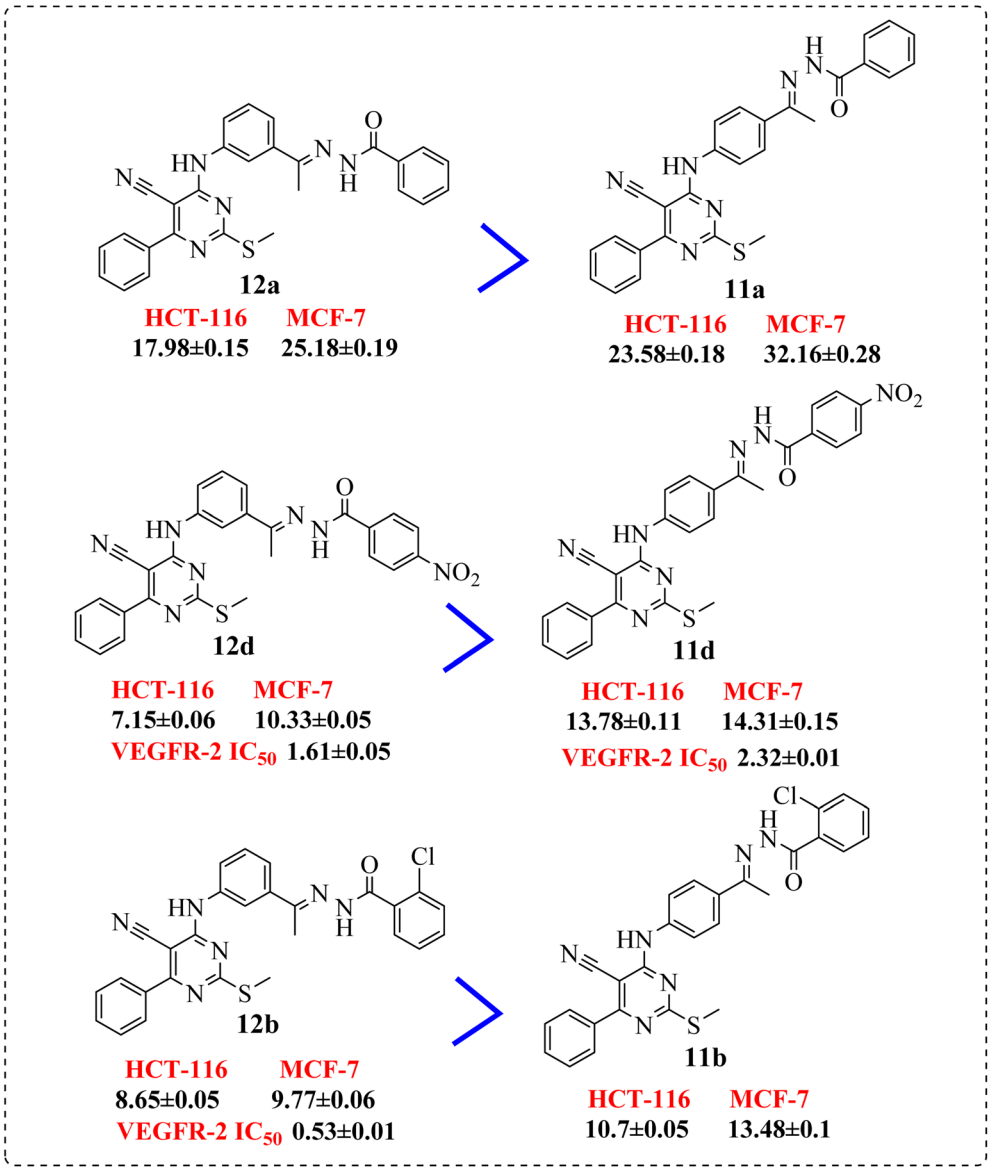

Fig. 3 SAR studies of **12a**, **12d**, and **12b** compared to **11a**, **11d**, and **11b**, respectively.

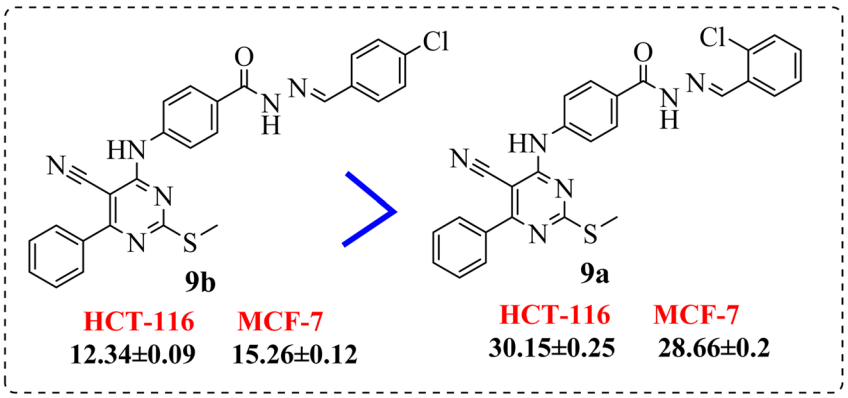

Fig. 4 SAR studies of **9b** compared to **9a**.

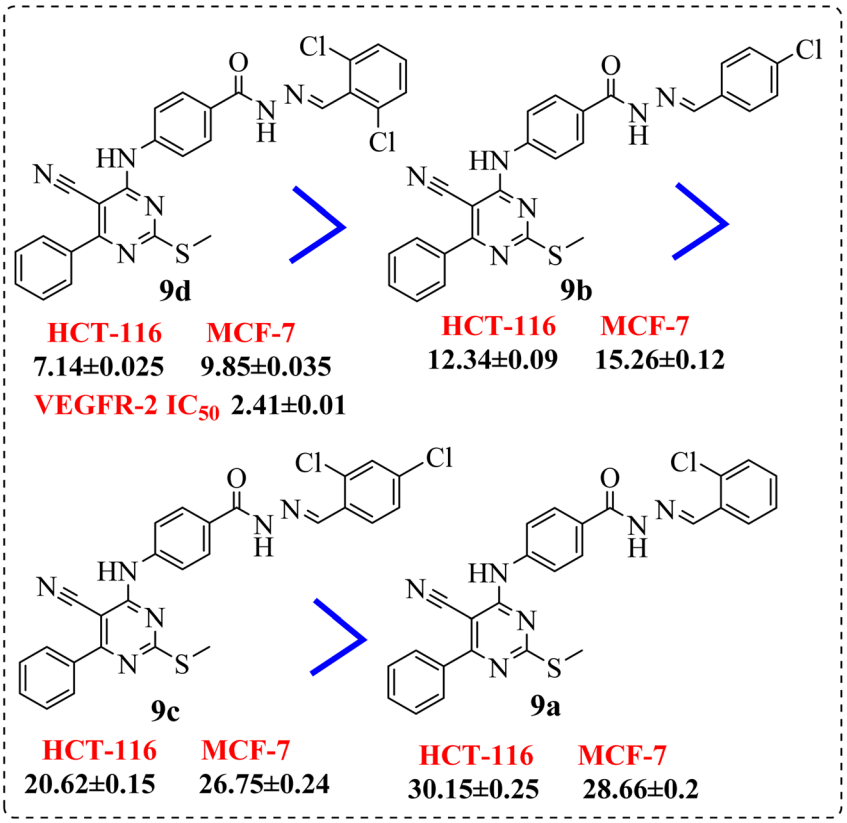

Fig. 5 SAR studies of **9d** and **9c** compared to **9b** and **9a**, respectively.

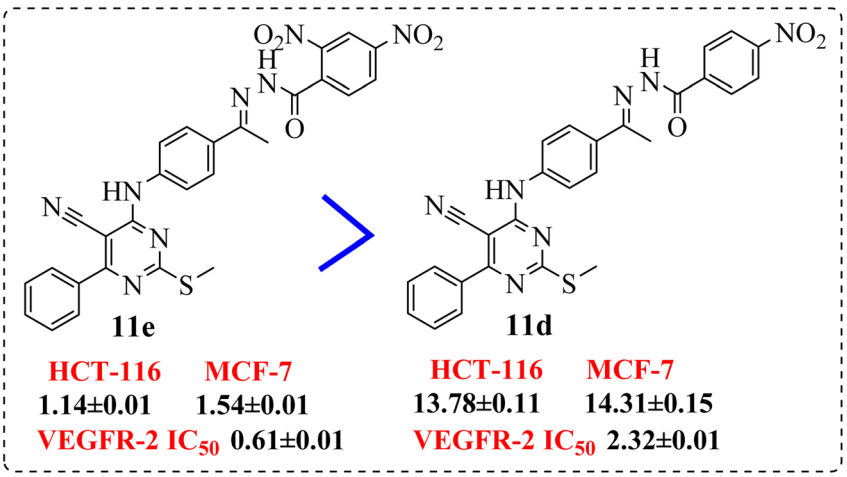

Fig. 6 SAR studies of **11e** compared to **11d**.

- Compounds **12b** and **12d**, containing terminal hydrophobic tail substituted with electron withdrawing groups with their corresponding derivatives with electron donating ones **12e** and **12g**, indicated the derivatives of electron withdrawing groups were more active than those donating one (Fig. 8).
- Introduction of electron withdrawing group at *o*-position and *m*-position exhibited preferable activity than *p*-position (Fig. 9).

2.2.5. Effect on cell cycle progression. To investigate the effect of the most promising compound **11e** on the various phases of the cell cycle in HCT-116 cells, flow cytometric analysis of cell cycle was performed using Epics XL-MCL™ Flow Cytometer[22,30] according to flow cytometric analysis technique.[31] The results obtained after exposure of HCT-116 cells to compound **11e** (as presented in Table 2, Fig. 10 and 11) indicated that the percentage of HCT-116 cells decreased at the G0/G1 and G2/M phases. For G0/G1 phase, it decreased from

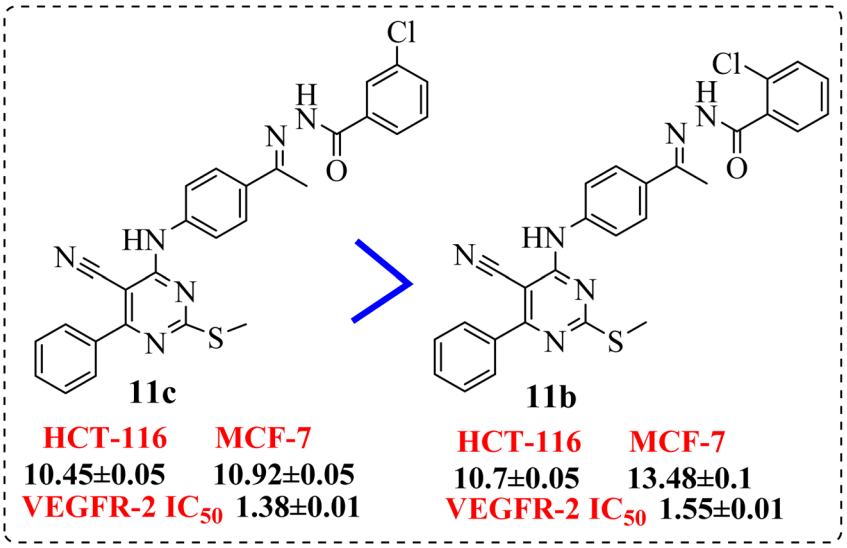

Fig. 7 SAR studies of **11c** compared to **11b**.

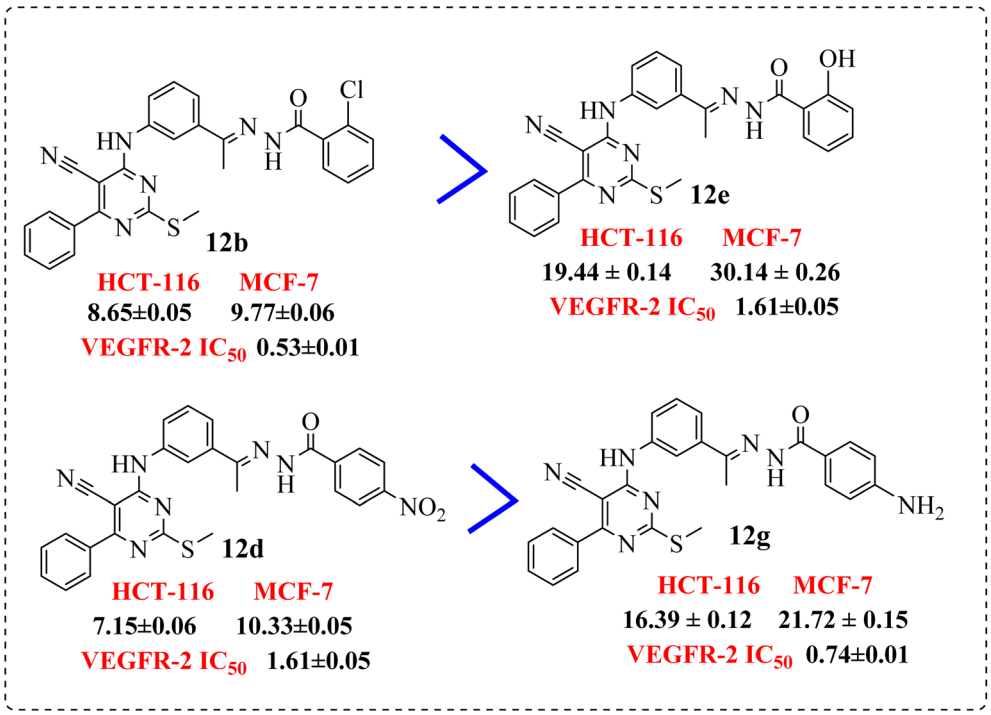

Fig. 8 SAR studies of **12b** and **12d** compared to **12e** and **12g**, respectively.

54.18% in control cells to 41.36%. At the G2/M phase, it decreased from 32.33% in the untreated cells to 22.43% in treated cells. On the contrary, the percentage of HCT-116 cells increased at Sub-G1 and S phases. For Sub-G1 phase, it increased from 2.70% in control cells to 21.36% (7.91-fold) in treated cells. For S phase, it increased from 13.49% in control cells to 36.21% (2.68-fold). These findings indicated that compound **11e** mainly arrested the cell cycle at S phase and induced apoptosis at Sub-G1 phase. Such findings were coordinated with the recorded results which established that the VEGFR-2 TK inhibitors can arrest the cell growth at S and Sub-G1 phases.[32]

2.2.6. Induction of apoptosis. Flow cytometry cell apoptosis analysis was used to investigate the apoptotic effect of the most active candidate on the treated HCT-116 cells. Apoptotic effect of compound **11e** on the treated HCT-116 cells was analyzed with the aid of annexin V-FITC-apoptosis detection kit (PN IM3546) using Epics XL-MCL™ Flow Cytometer.[30,33] The results of apoptosis induction (as represented in Table 3, Fig. 12 and 13) indicated that exposure of

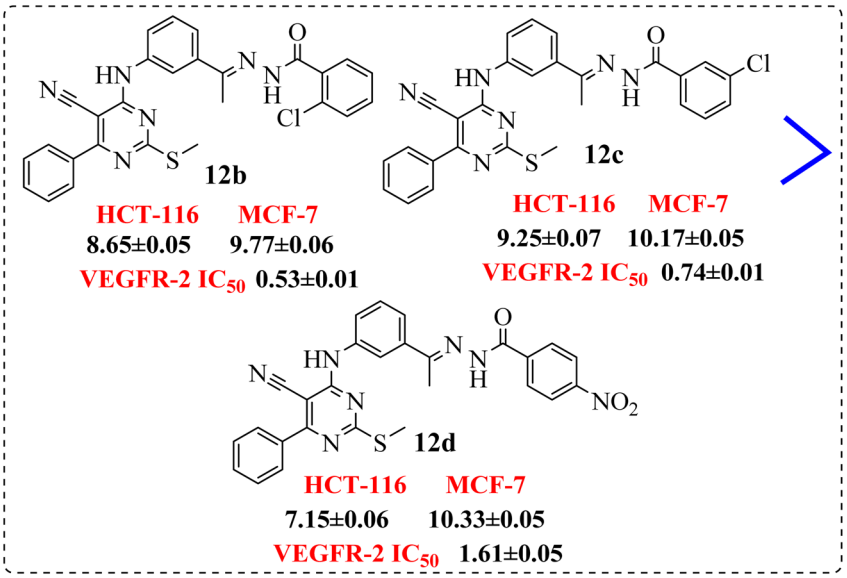

Fig. 9 SAR studies of **12b** and **12c** compared to **12d**.

Table 2 Effect of compound **11e** on cell cycle progression in HCT-116 cells

	Cell cycle distribution[a] (%)			
Sample	% Sub-G1	% G0/G1	% S	% G2/M
Cont./HCT-116	2.70	54.18	13.49	32.33
Compound **11e**/HCT-116	21.36	41.36	36.21	22.43

[a] Values are given as mean of twice independent experiments.

HCT-116 cells to compound **11e** resulted in a significant increase in the percentage of apoptotic cells in the early stage from 0.85% (untreated control cells) to 5.47%. Furthermore, in the late phase, there was an increase in the apoptotic cells to attain 15.70% in comparison to 1.31% in control HCT-116 cells.

2.2.7. *In vitro* immunomodulatory assay of TNF-α and IL-6. The selected compound **11e**, was further evaluated for its effects on the expression levels of TNF-α and IL-6 in HCT-116 cell line. Dexamethasone was used as positive controls as included in literature.[8] The effects of compound **11e** on the expression of TNF-α and IL-6 were determined using qRTPCR technique.[34] The quantity of immunomodulatory proteins (TNF-α and IL-6) in control and compound **11e** (at the IC_{50} concentration)-treated HCT-116 cells was assessed by qRTPCR (reference).

In these experiments, we calculated the changes in the expression levels of such proteins that resulted from the treatment of HCT-116 cells for 24 h with the selected molecule at their IC_{50}. The data outlined in (Table 4) showed the

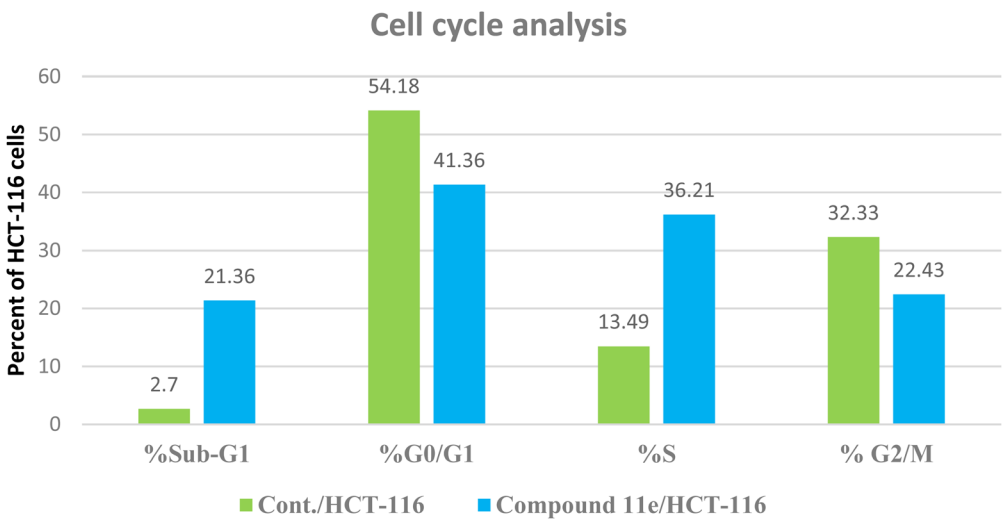

Fig. 10 The representative histograms show the cell cycle distribution of control (HCT-116), and cells treated with compound **11e**.

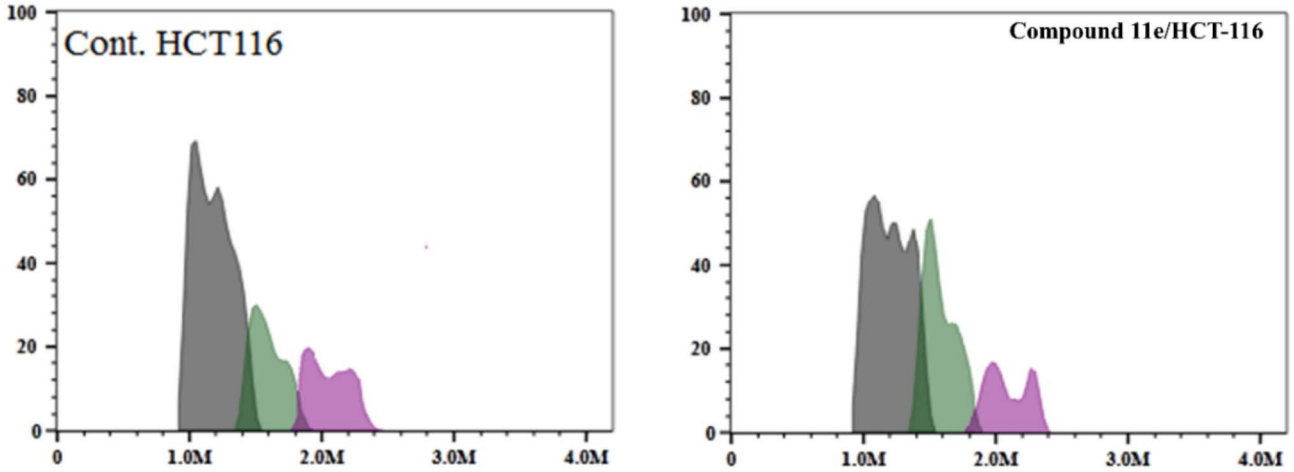

Fig. 11 Flow cytometric analysis of cell cycle phases post the compound **11e** treatment.

Table 3 Effect of compound **11e** on stages of the cell death process in HCT-116 cells

		Apoptosis[a]		
Sample	Viable[a] (left bottom)	Early (right top)	Late (right bottom)	Necrosis[a] (left top)
Cont./HCT-116	97.30	0.85	1.31	0.54
Comp. **11e**/HCT-116	78.64	5.47	15.70	0.19

[a] Values are given as mean of twice independent experiments.

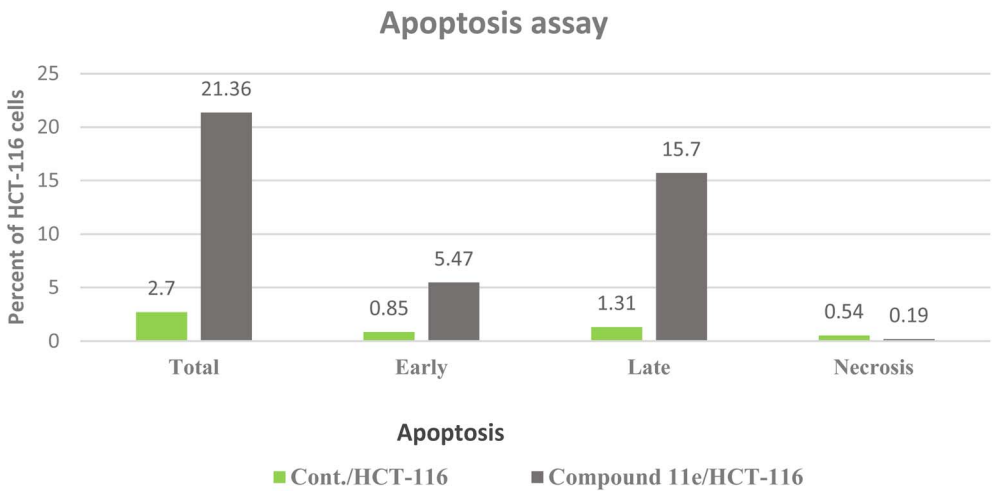

Fig. 12 The representative flow cytometric charts for control (HCT-116) and the cells treated with compound **11e**.

significance of compound **11e** as potent inhibitor for the pro-inflammatory factors TNF-α and IL-6, which played main role in immunomodulatory activity (Fig. 14). Compound **11e** caused remarkable decrease in the levels of TNF-α and IL-6, with inhibition percent 70.22 pg per mL % for TNF-α & 81.39, 79.52 and 84.46 pg per mL % for IL-6, respectively.

2.2.8. *In vitro* assessment of caspase-3 expression. The effect of the selected candidate **11e** on the expression level of caspase-3 in HCT-116 cells was evaluated in comparison to HCT-116 cells treated with DMSO represented as a negative control. As can be seen from (Table 5), the tested molecule was comparable to control in its effects on caspase-3 levels. Compound **11e** showed a notable increase in caspase-3 concentration (304.67 pg mL^{-1}) by 5.4 folds, compared to the negative control (see Fig. 15).

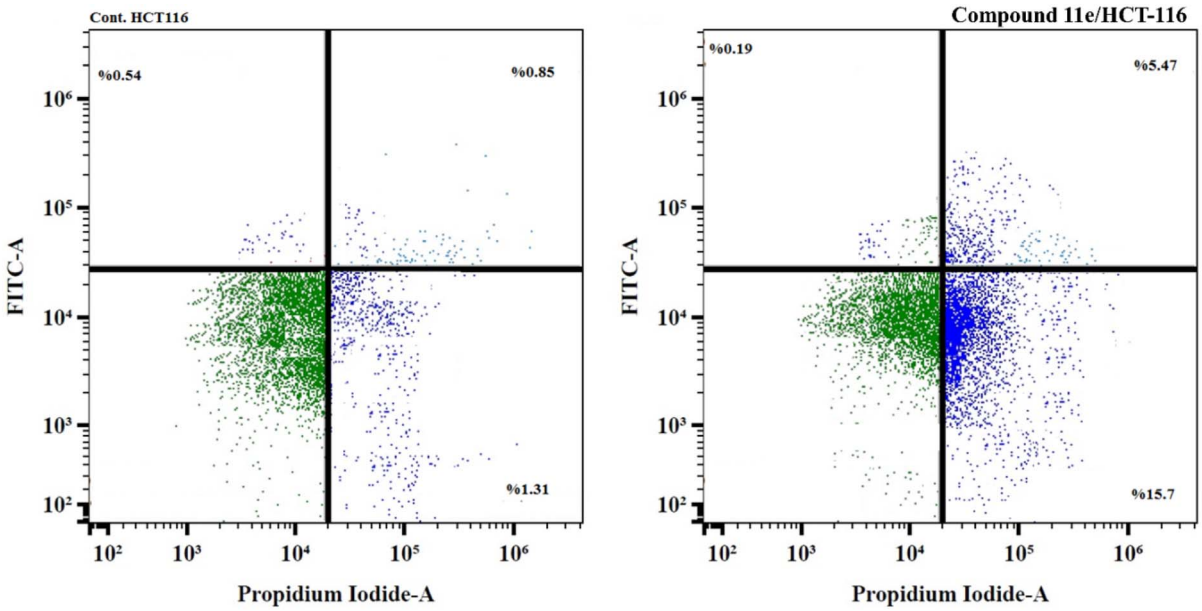

Fig. 13 Flow cytometric analysis of apoptosis in HCT-116 cells exposed to compound **11e**. For each dot plot chart, the quadrant regions represent the cells in each sub-population; lower left quadrant (viable cells), lower right quadrant (late apoptosis), upper right quadrant (early apoptosis), and upper left quadrant (necrosis).

Table 4 Immunomodulatory assay of the compound **11e** against the pro-inflammatory factors TNF-α and IL-6

	Pro-inflammatory factors inhibition (pg per mL %)	
Sample	TNF-α	IL-6
Dexamethasone	82.47	93.15
Compound **11e**/HCT-116	70.22	84.46

2.3. *In silico* studies

2.3.1. Docking study. Docking study was performed to get insight into how the designed compounds could bind to the ATP binding site of VEGFR-2 TK and inhibit its downstream signaling pathways. The results of these studies could help us to understand the binding modes of the target compounds with the crucial amino acids in the ATP binding site of VEGFR-2 TK (Table 6). In these studies, the free energies, and binding modes of the designed molecules against the VEGFR-2 TK active site were determined. Molecular Operating Environment (MOE 19.0102) software was used for the docking analysis and Biovia discovery studio 2016 was used for the visualization. Validation of the docking protocol was performed through the re-docking of the co-crystalized ligand inside the active site of VEGFR-2 TK. The resulted RMSD between the re-docked and the co-crystallized ligand was 0.49 Å which indicated the validity of the docking protocol (Fig. 16).

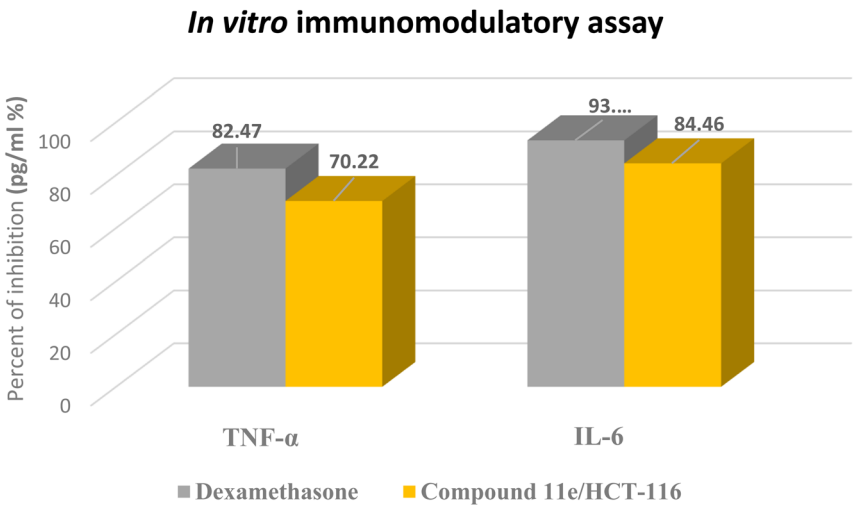

Fig. 14 The representative *in vitro* immunomodulatory assay charts for dexamethasone as positive control and the tested compound **11e**.

Table 5 Caspase-3 expression analysis of the tested compound **11e** as apoptotic inducer

	Apoptosis markers assay (pg mL^{-1})	
Sample	Caspase-3	Fold
Cont./HCT-116	56.48	1
Compound **11e**/HCT-116	304.67	5.4

Table 6 The calculated Δ*G* (binding free energies) of the synthesized compounds and reference drug against VEGFR-2 TK (Δ*G* in kcal mol^{-1})

Comp.	Δ*G* [kcal mol^{-1}]	Comp.	Δ*G* [kcal mol^{-1}]
9a	−8.70	**12a**	−8.95
9b	−8.23	**12b**	−9.17
9c	−8.95	**12c**	−8.99
9d	−8.85	**12d**	−9.01
11a	−9.32	**12e**	−9.34
11b	−8.82	**12f**	−8.60
11c	−9.06	**12g**	−8.90
11d	−9.30	Sorafenib	−8.70
11e	−9.36		

The native ligand was exhibited an affinity score of −10.90 kcal mol^{-1} with RMSD value equal 0.49 Å (Fig. 17). It showed many important interactions with the residues at the active site of VEGFR-2 TK. The urea side chain possessed both hydrogen bond acceptor and donor, which bound with two crucial residues (Glu883 and Asp1044) of the receptor, where the NH motifs of the urea moiety usually formed two hydrogen bonds with the carboxylate of Glu883 with distance of 2.01 and 1.94 Å. Whereas the C=O motif formed another hydrogen bond with the backbone NH of with Asp1044 with a distance of 2.05 Å at DFG region. The heterocyclic moiety showed two extra hydrogen bonds with Glu915 and Cys917. Besides, the phenyl group (spacer) interacted with the hydrophobic site (Val914, Ala864, Cys1043 and Val846) in the linker region by pi interactions. These results were found to be identical to the reported data.[35]

Sorafenib interactions with the amino acids of the pocket have been studied and displayed in 2D and 3D style in (Fig. 18). The proposed binding mode of sorafenib, revealed an affinity value of −8.70 kcal mol^{-1}. It demonstrated the important interactions with the residues at the active site of VEGFR-2 TK. The urea moiety possessed both hydrogen bond acceptor and donor that bound with two crucial residues (Glu883 and Asp1044) of the receptor, where the NH motifs of the urea moiety formed two hydrogen bonds with the carboxylate of Glu883 with distances of 2.02 and 1.98 Å. Whereas the C=O motif formed another hydrogen bond with the backbone NH of with Asp1044 with a distance of 2.03 Å at DFG region. Besides, the phenyl group (spacer) interacted with the hydrophobic site (Cys917, Cys1043 and Phe916) in the linker region. Moreover, the distal hydrophobic moiety attached to the urea linker occupied the hydrophobic pocket formed by Cys1043, Val896,

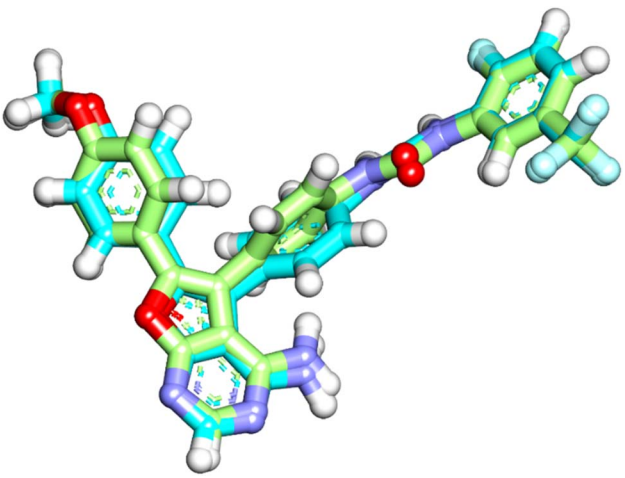

Fig. 16 Superimposition of the native ligand (turquoise) and the re-docked one (green) in the VEGFR-2 TK active site (RMSD = 0.49 Å).

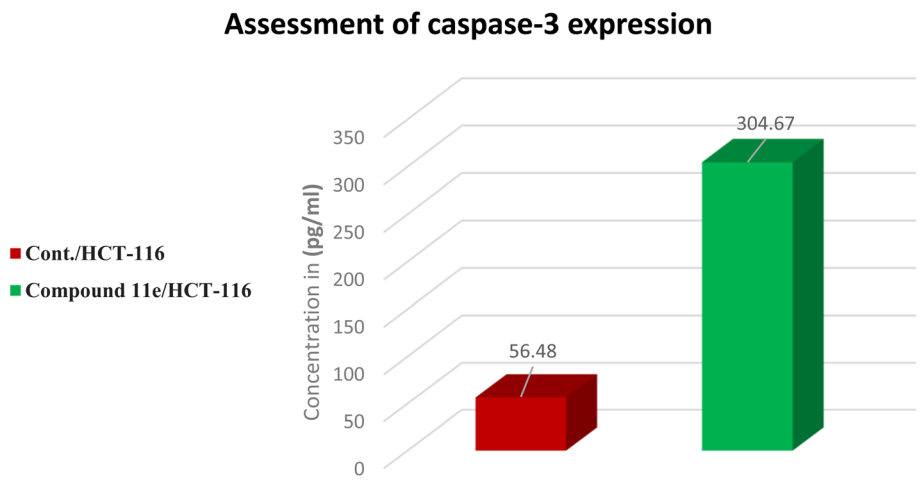

Fig. 15 The representative *in vitro* caspase-3 expression chart for the tested compound **11e**.

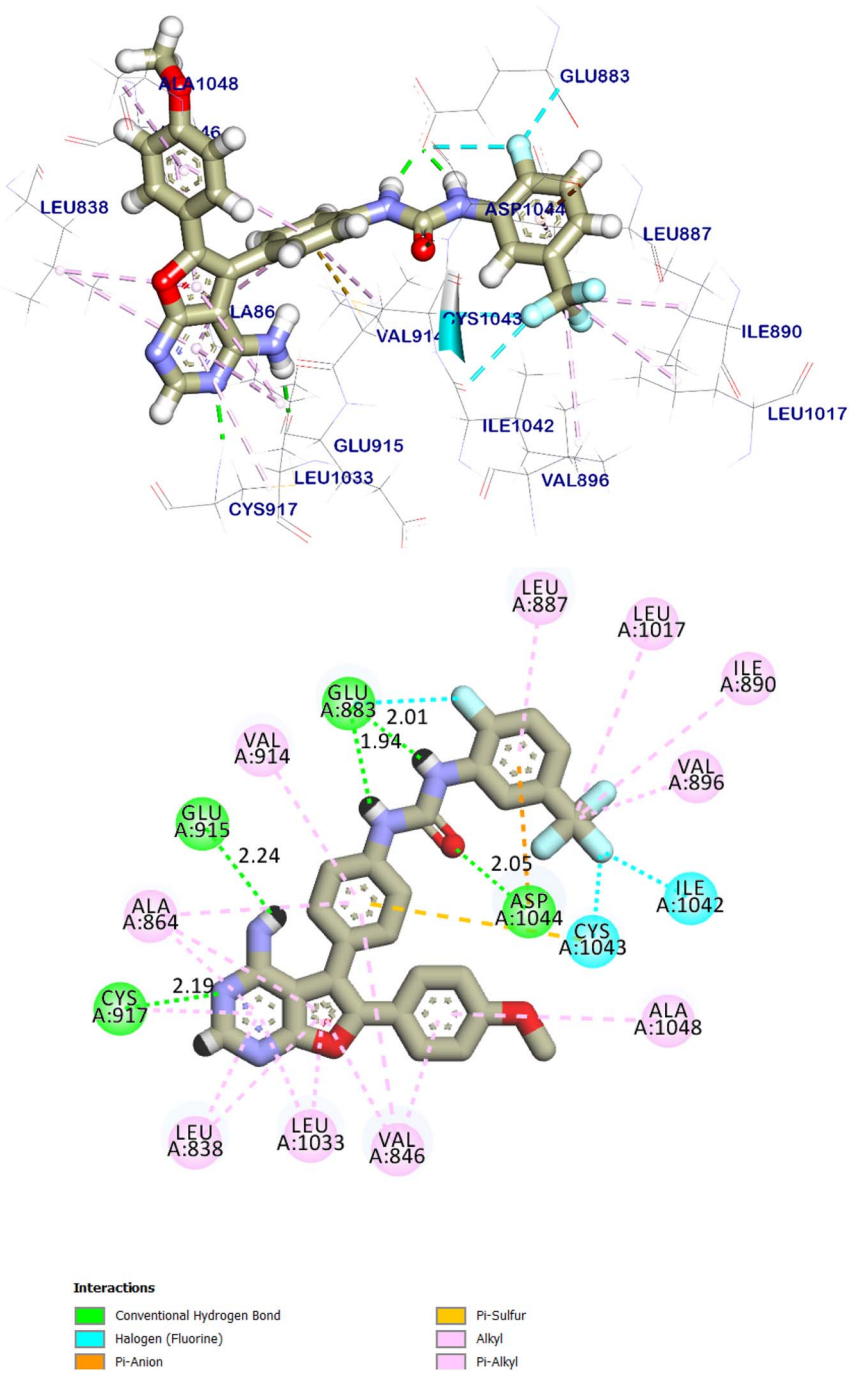

Fig. 17 The predicted binding mode for the co-crystalized ligand with the active site of VEGFR-2 TK.

Asp1044, Ile886, Ile890, Ile1042, and Leu887. Furthermore, the *N*-methylpicolinamide moiety occupied the hinge region, it was formed one hydrogen bond with Cys917 with a distance of 2.79 Å and pi interactions with Ala864, Phe916, Leu838, Leu1033 and Cys917 (Fig. 18). The urea linker played an important role in the binding affinity towards VEGFR-2 TK, which was responsible for the higher binding affinity of sorafenib. These results were found to be identical to the reported data.[36]

The docking score for compound **9d** was −8.85 kcal mol^{-1}. Through its pharmacophoric group, it formed two hydrogen bonds with Glu883 and Asp1044. The spacer moiety (4-amino-phenyl ethylidene) interacted hydrophobically with Val914, and Cys1043. Many hydrophobic interactions in the hinge region occurred between the 5-cyano-2-(methylthio)-6-phenyl-pyrimidin moiety and different amino acid residues including Leu838, Val846, Gly1046, Phe843, and Ala1048. Furthermore, in

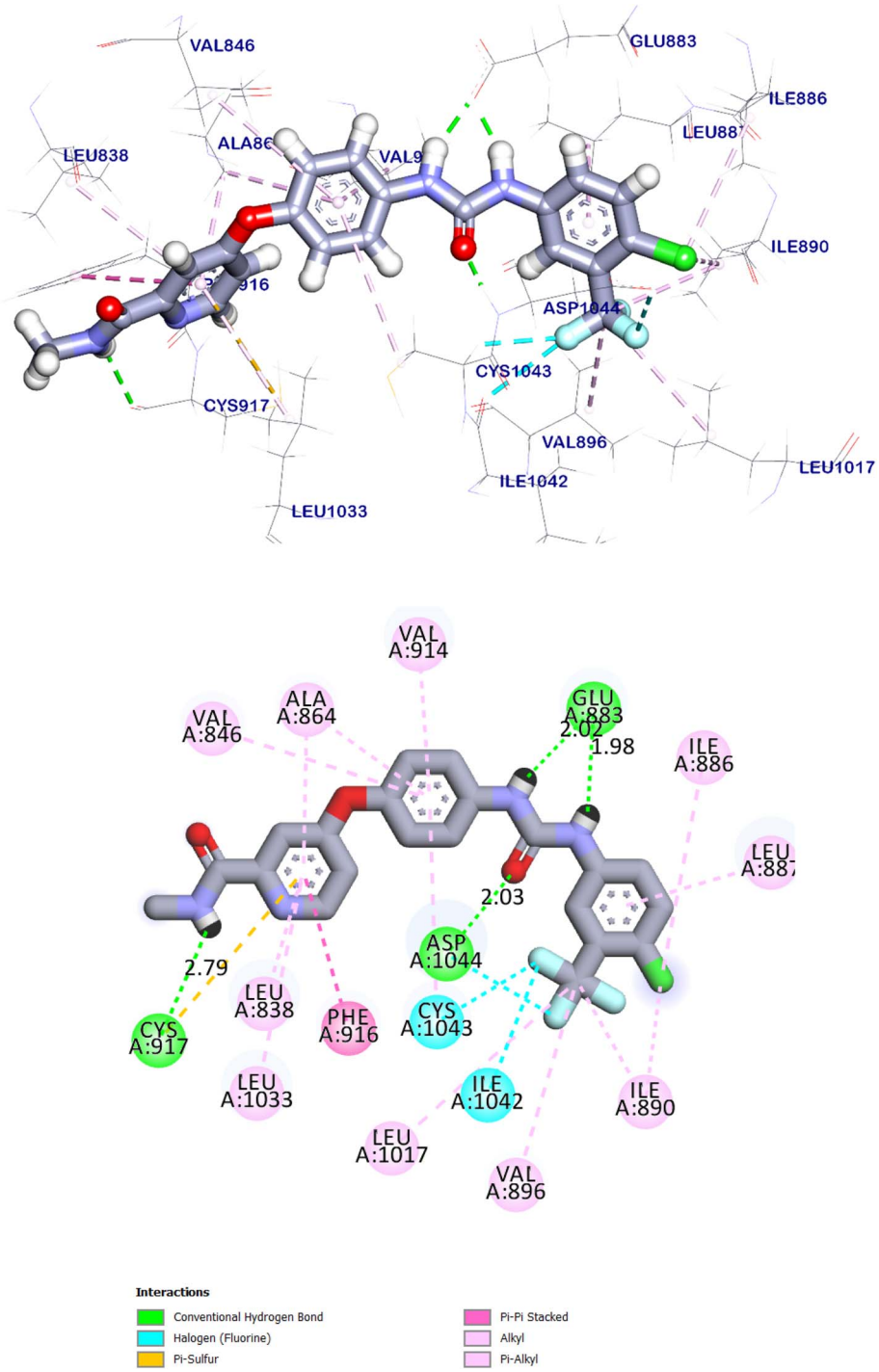

Fig. 18 The predicted binding mode for sorafenib with the active site of VEGFR-2 TK.

the allosteric pocket, the 2,6-dichloro phenyl group formed numerous hydrophobic interactions with Val896, Val897, Ile890, Ile886, Phe1045 and Leu887. It also had a pi–anion interaction with Asp1044 (Fig. 19).

The docking findings of compound **11e** revealed that it can interact with the essential amino acids in the VEGFR-2 TK active site. As displayed in (Fig. 20), it was showed docking energy of −9.36 kcal mol^{-1}. Both 4-amino phenyl and 5-cyano-2-(methylthio)-6-phenylpyrimidin moieties were oriented towards the gate keeper area and the hinge region, respectively, which bound with Ala1048 and Arg1049 by two hydrogen bonds with distances 2.75 and 2.80 Å, additionally, it was interacted with Val846, Ala864, Lys866, Val914, Cys1043, Ala1048 and Arg1049 by seven hydrophobic interactions. Also, compound **11e** incorporated in two hydrogen bonds with the key amino acids; Glu883 (2.18 Å) and Asp1044 (2.52 Å) in the DFG motif.

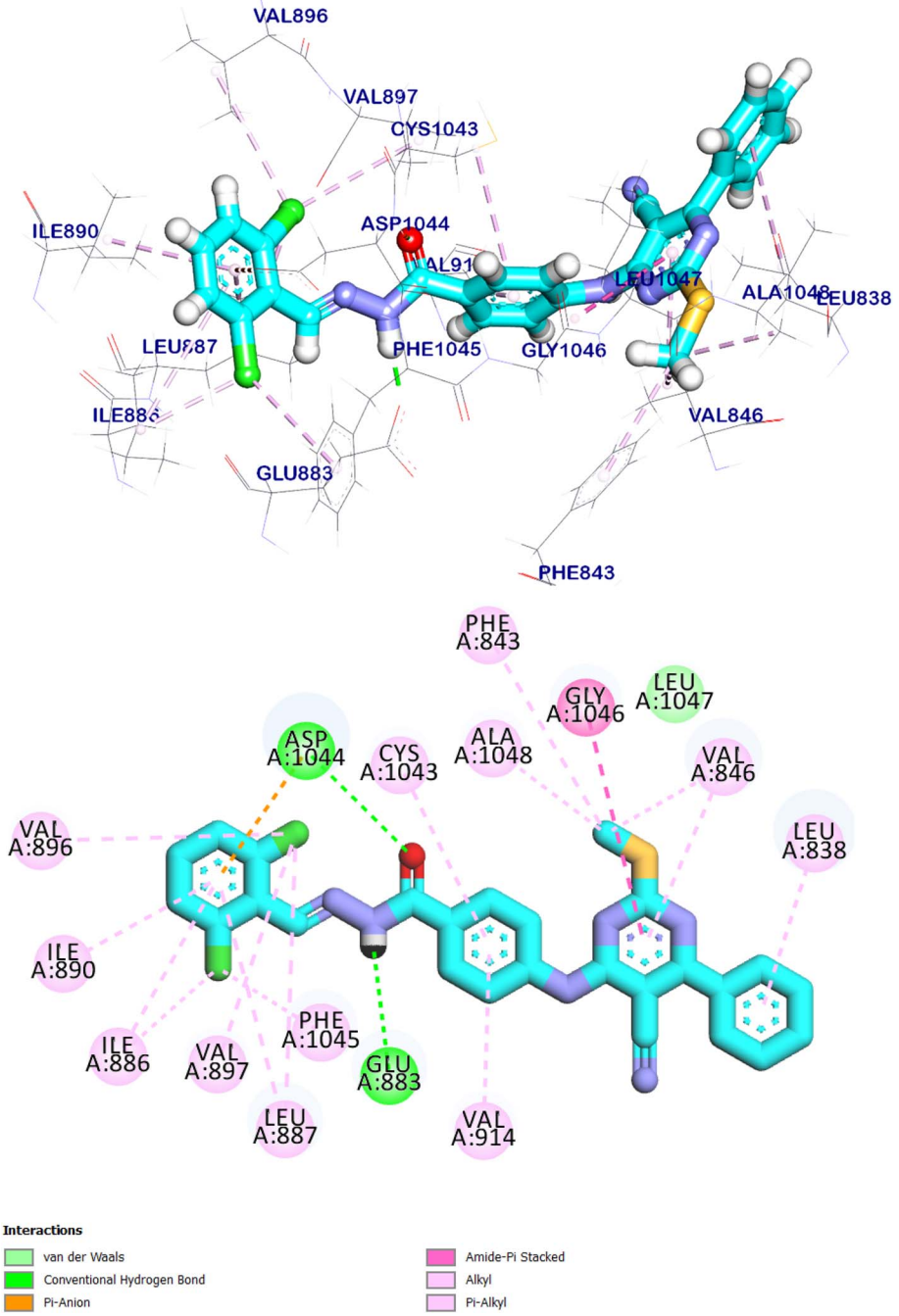

Fig. 19 The predicted binding mode of compound **9d** with the active site of VEGFR-2 TK.

Additionally, the of the later moieties' orientation allowed the hydrophobic substituents in the docked compound to fit inside the hydrophobic allosteric pocket. Such a binding pattern of compound **11e** encouraged us to study its MD simulation.

Compound **12a** showed docking energy of −8.95 kcal mol^{-1}. The 5-cyano-2-(methylthio)-6-phenylpyrimidin moiety formed seven hydrophobic interactions in the hinge region with Arg1049, Ala1048, Leu1047, Leu1033, and Cys1043. Additionally, it was formed two hydrogen bonds with Arg1049 and Arg1030. The 4-amino phenyl (linker) moiety formed an extra hydrogen bond with Gly1046 in addition to two hydrophobic interactions with Val846, and Ala864. The pharmacophore moiety occupied the DFG region forming two hydrogen bonds with Glu883 Asp1044. The terminal hydrophobic moiety occupied the allosteric pocket forming four hydrophobic interactions with Leu887, Lys866, Asp1044, and Val917 (Fig. 21).

The net result of computational studies of the designed molecules indicates that most of the synthesized compounds showed significant VEGFR-2 TK inhibition affinities.

Comparing to the binding modes of the reference drugs, we found a lot of compounds have excellent binding modes with ΔG values higher than or at least similar to that of the reference

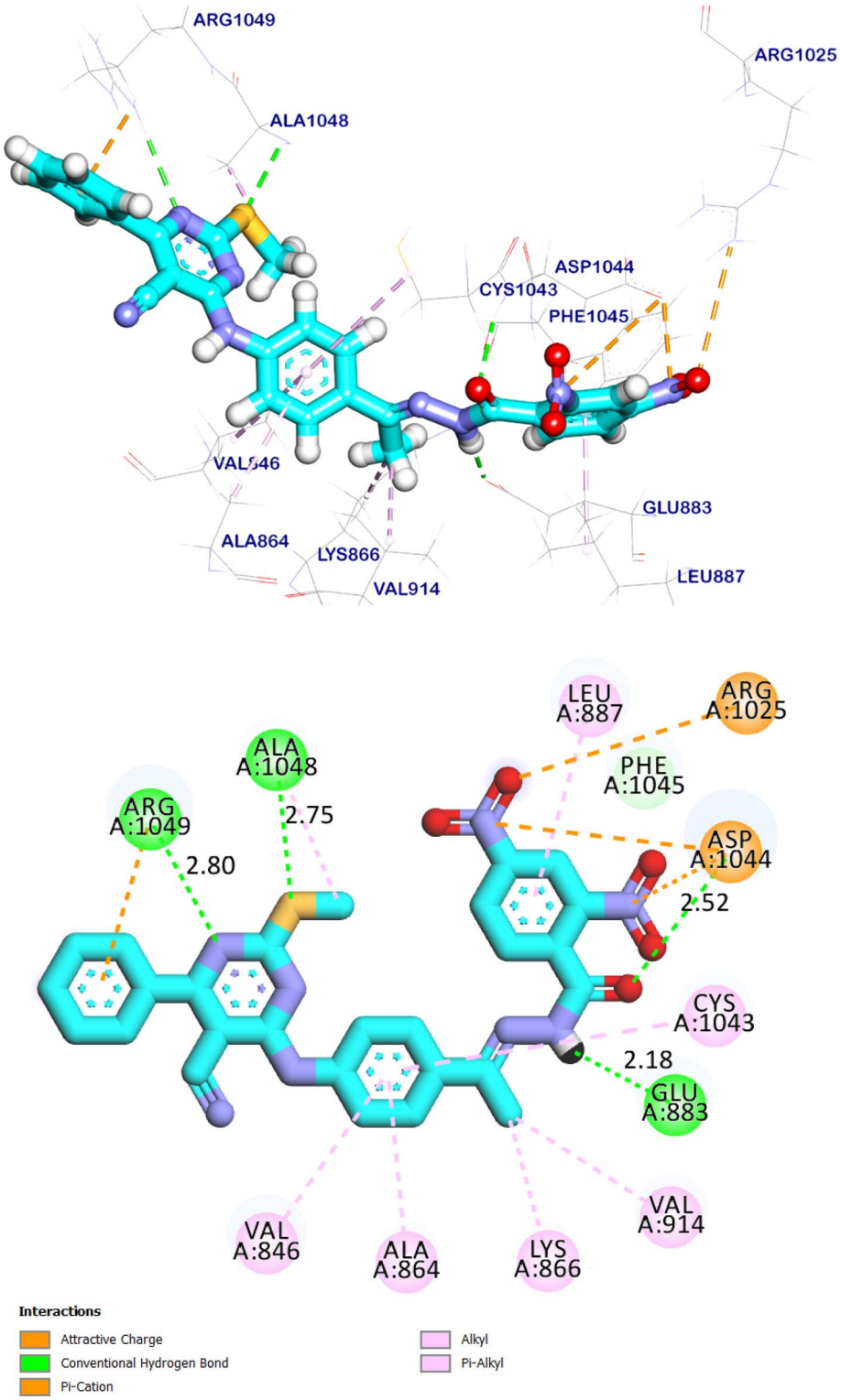

Fig. 20 The predicted binding mode of compound **11e** with the active site of VEGFR-2 TK.

drugs (sorafenib), against VEGFR-2 TK with ΔG values ranging from −8.23 to −9.36 compared with sorafenib ΔG value −8.70. Other compounds showed binding affinities lower than that of the reference drugs. The results may give guidance for further structural modifications.

The *p*-di-substituted and *m*-di-substituted benzohydrazide derivatives **11a–e** and **12a–g** exhibited a higher ability to form hydrogen bonds interaction than other groups, which explains their higher cytotoxic activity. Specifically, compounds with benzohydrazide side chains, such as **11e**, **11b**, **11d**, **11c**, **12b**,

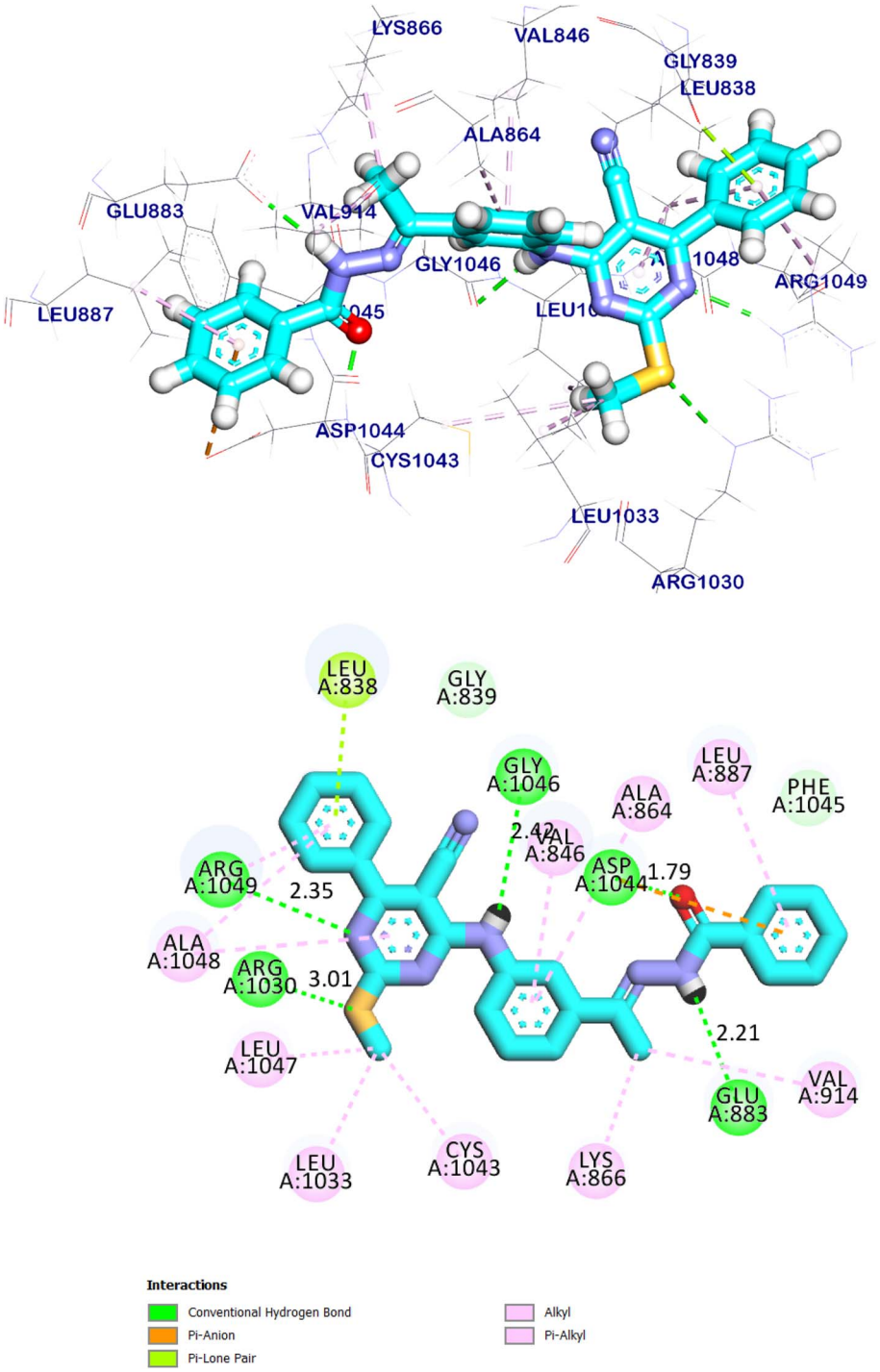

Fig. 21 The predicted binding mode of compound **12a** with the active site of VEGFR-2 TK.

12d, and **12c**, showed high affinity toward VEGFR-2 TK with (ΔG −9.36, −8.82, −9.30, −9.06, −9.17, −9.01, and −8.99), respectively, and these results were consistent with the cytotoxicity MTT assay. Furthermore, the series with a benzylidene side chain exhibited a remarkable affinity score against VEGFR-2 TK, such as compounds **9c** which had affinity score (−8.95 kcal mol^{-1}) higher than sorafenib (−8.70 kcal mol^{-1}).

2.3.2. Molecular dynamic (MD) simulations. The dynamic movements of atoms and conformational variations of backbone atoms of the protein–ligand complex were calculated by RMSD to detect their stability upon apo and ligand bonded state. It was observed that the protein, ligand, and the complex exhibited a lower RMSD values with no major fluctuations throughout the simulation, indicating their greater stability.

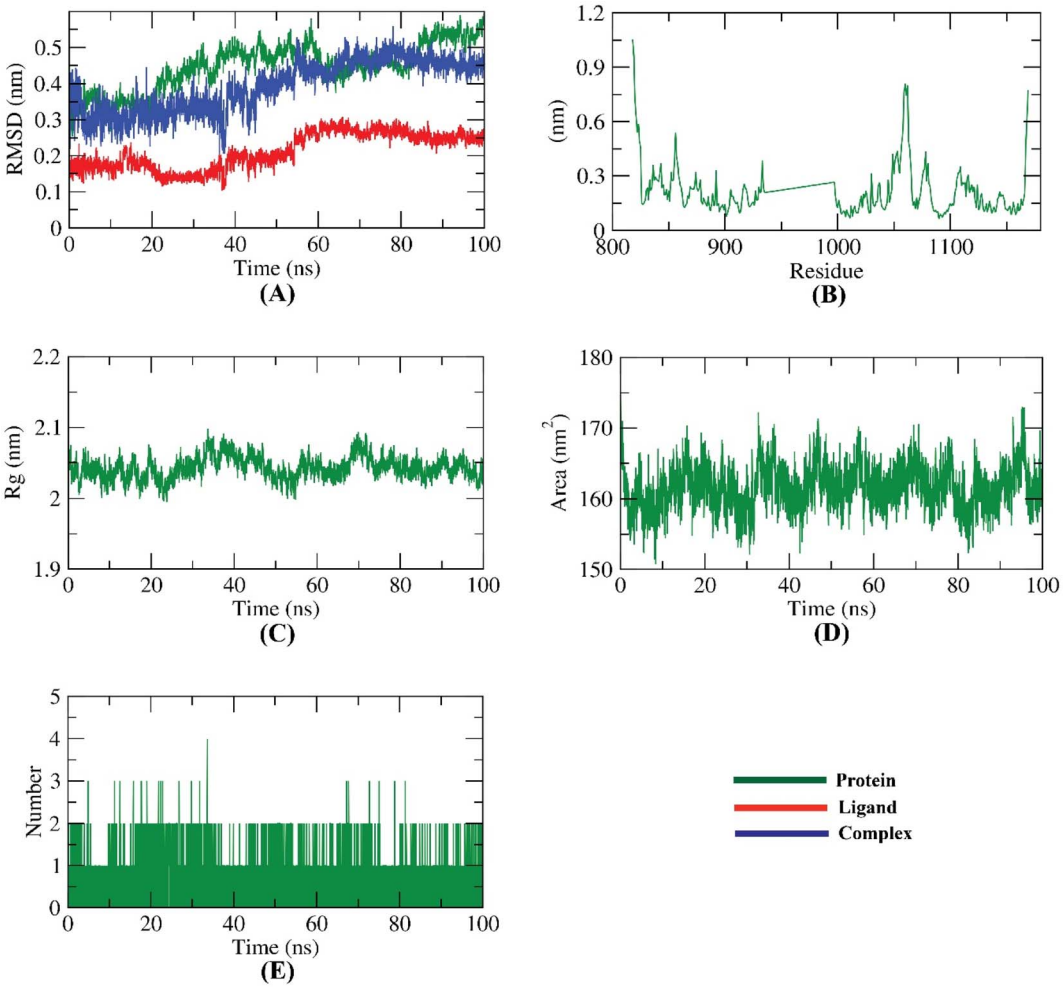

Fig. 22 MD simulations; (A) RMSD, (B) RMSF (C) R_g (D) SASA, and (E) hydrogen bonding for compound **11e**-VEGFR-2 TK complex over the MD run (100 ns).

The flexibility of each residue was calculated in terms of RMSF to get better insight on the region of proteins that are being fluctuated during the simulation. It can be understood that the binding of ligand makes the protein flexible in 1025–1075 residue areas. The compactness of the complex was represented by the radius of gyration (R_g). The lower degree of fluctuation throughout the simulation period indicates the greater compactness of a system. The R_g of the complex was found to be similar compared to the starting period. Interaction between protein–ligand complexes and solvents was measured by solvent accessible surface area (SASA) over the simulation period. So, SASA of the complex was calculated to analyze the extent of the conformational changes occurred during the interaction. Interestingly, the protein featured neither reduction nor expansion of the surface area showing relatively similar SASA value than the starting period. Hydrogen bonding between a protein–ligand complex is essential to stabilize the structure. It was observed that the highest number of conformations of the protein formed up to two hydrogen bonds with the ligand (Fig. 22).

2.3.3. Molecular mechanics Poisson–Boltzmann surface area (MM-PBSA). We calculated the binding free energy of the last 20 ns of MD production run of the protein–ligand complex with an interval of 100 ps from MD trajectories using MM/PBSA method. We also utilized the MmPbSaStat.py script that calculated the average free binding energy and its standard deviation/error from the output files that were obtained from g_mmpbsa. The ligand showed binding free energy of −139 kJ mol^{-1} with the protein. Further, we identified the contribution of each residue of the protein in terms of binding free energy to the interaction with the ligand. By decomposing the total binding free energy of the system into per residue contribution energy, the contribution of each residue was calculated. This gave us an insight into the 'crucial' residues that contributes favorably to the binding of this molecule to the protein. It was found that Leu838, Val846, Ala864, Ile886, Leu887, Val897, Val914 and Leu1033 residues of the protein contributed higher than −5 kJ mol^{-1} binding energy and thereby are hotspot residues in binding with the ligand (Fig. 23).

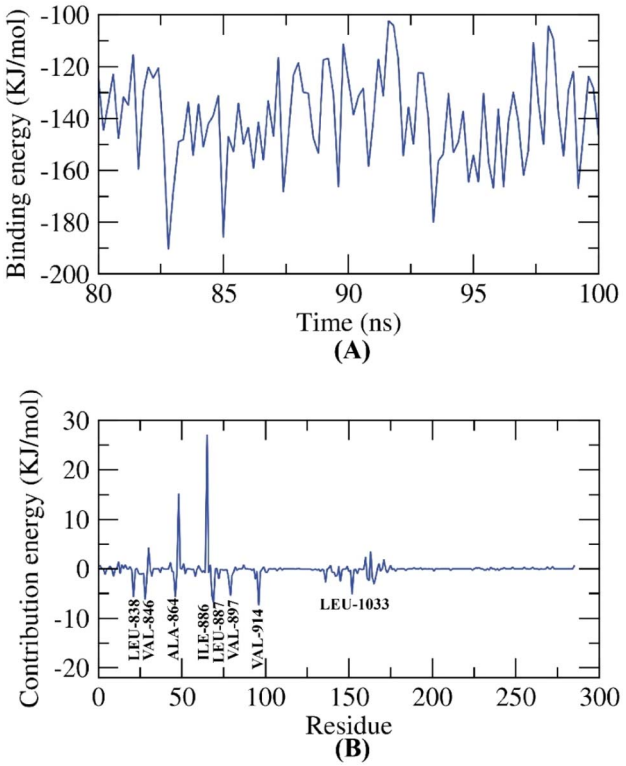

Fig. 23 MM-PBSA outputs of the compound **11e**-VEGFR-2 TK complex.

3. Conclusion

A new sixteen pyrimidine-5-carbonitrile derivatives were designed and synthesized as VEGFR-2 TK inhibitors. The synthesized compounds were evaluated *in vitro* for their anti-proliferative activities against colon cancer (HCT-116), and breast cancer (MCF-7) cell lines. Compounds **9b**, **9d**, **11b**, **11c**, **11e**, **12b**, **12c**, and **12d** exhibited the highest activities towards both cell lines. In particular, compound **11e** exhibited the best cytotoxic activity against HCT-116 and MCF-7 with IC_{50} values of 1.14 ± 0.01 and 1.54 ± 0.01 μM, respectively, compared to sorafenib as a reference drug with IC_{50} values of 8.96 ± 0.05 & 11.83 ± 0.07 μM, respectively. In addition, the most active cytotoxic agents **11e** was further assessed for their inhibitory action on VEGFR-2 TK activity to confirm the mechanism responsible for their induced cytotoxic activities. The *in vitro* analysis of VEGFR-2 TK inhibition revealed that, compounds **11e** and **12b** were the most potent VEGFR-2 TK inhibitors with an IC_{50} values of 0.61 ± 0.01 and 0.53 ± 0.07 μM, respectively, in comparing with that of sorafenib (IC_{50} = 0.19 ± 0.15 μM). Moreover, compound **11e** arrested the cell growth in HCT-116 cells at S and sub-G1 phase and induced a significant increase in the apoptotic cells. Finally, the binding patterns of the target derivatives were investigated through the docking study against the proposed molecular target (VEGFR-2 TK, PDB ID 1YWN). The results of molecular docking studies showed similar binding modes and interactions to sorafenib against VEGFR-2 TK active site.

4. Experimental

4.1. Chemistry

Compounds, 4-oxo-6-phenyl-2-thioxo-1,2,3,4-tetrahydropyrimidine-5-carbonitrile **1**,[21,22] 2-(methylthio)-6-oxo-4-phenyl-1,6-dihydro-pyrimidine-5-carbonitrile **2**,[37] 4-chloro-2-(methylthio)-6-phenylpyrimidine-5-carbonitrile **3**,[37] substitutedbenzohydrazide **10a–e**[24,38–40] were prepared according to the reported procedures.

4.1.1. General procedure for the synthesis of compounds 4, 5 & 6. To a solution of compound **3** (2.61 g, 0.01 mol) in *n*-butanol (15 mL) containing few drops of TEA, the appropriates amines namely *p*-amino benzoic acid, *p*-amino acetophenone, and *m*-amino acetophenone (0.01 mol) were added. The mixture was heated under reflux for sufficient time. After completion of reaction (monitored using TLC), the reaction mixture was concentrated, cooled, and poured onto ice water (50 mL). Then, the solution was acidified with dil. HCl with continuous stirring for 15 min. The formed precipitate was filtered, washed with water several times and dried. The cropped powder was crystallized from ethanol to afford the target compounds **4**, **5**, & **6**, respectively.

*4.1.1.1. 4-[(5-Cyano-2-(methylthio)-6-phenylpyrimidin-4-yl) amino]benzoic acid **4**.* Off-white powder (yield 83.4%, 3.1 g); mp = 273–274 °C; IR (KBr) ν cm^{-1}: 3451 (OH), 3319 (NH), 2975 (CH aromatic), 2928 (CH aliphatic), 2210 (C≡N), 1696 (C=O), 1614 (C=N); ^{1}H NMR (400 MHz, DMSO-d_6) δ ppm: 12.85 (s, 1H, OH), 10.12 (s, 1H, NH), 7.96 (d, J = 8.5 Hz, 2H, Ar–H, H-3 & H-5 of –C_6H_4), 7.90 (d, J = 6.5 Hz, 2H, Ar–H, H-2 & H-6 of –C_6H_5), 7.79 (d, J = 8.5 Hz, 2H, Ar–H, H-2 & H-6 of –C_6H_4), 7.65–7.57 (m, 3H, Ar–H, H-3, H-4 & H-5 of –C_6H_5), 2.51 (s, 3H, SCH_3); ^{13}C NMR (101 MHz, DMSO-d_6) δ ppm: 174.72, 168.71, 167.38, 160.39, 142.53, 136.24, 131.78, 130.24 (2C), 129.25 (2C), 129.06 (2C), 126.81, 122.93 (2C), 116.40, 85.84, 14.30; molecular formula $C_{19}H_{14}N_4O_2S$ (362.41).

*4.1.1.2. 4-[(4-Acetylphenyl)amino]-2-(methylthio)-6-phenylpyrimidine-5-carbonitrile **5**.* Beige fluffy powder (yield 93.5%, 3.36 g); mp = 236–235 °C; ^{1}H NMR (400 MHz, DMSO-d_6) δ ppm: 10.15 (s, 1H, NH), 7.99 (d, J = 8.5 Hz, 2H, Ar–H, H-3 & H-5 of –C_6H_4), 7.90 (d, J = 6.2 Hz, 2H, Ar–H, H-2 & H-6 of –C_6H_5), 7.83 (d, J = 8.4 Hz, 2H, Ar–H, H-2 & H-6 of –C_6H_4), 7.66–7.58 (m, 3H, Ar–H, H-3, H-4 & H-5 of –C_6H_5), 2.58 (s, 3H, $COCH_3$), 2.52 (s, 3H, SCH_3); ^{13}C NMR (101 MHz, DMSO-d_6) δ ppm: 197.21, 174.73, 168.73, 160.34, 142.88, 136.23, 133.11, 131.80, 129.30 (2C), 129.26 (2C), 129.07 (2C), 122.73 (2C), 116.40, 85.99, 27.05, 14.34; molecular formula $C_{20}H_{16}N_4OS$ (360.44).

*4.1.1.3. 4-[(3-Acetylphenyl)amino]-2-(methylthio)-6-phenylpyrimidine-5-carbonitrile **6**.* Faint brown fluffy powder (yield 93.4%, 3.36 g); mp = 226–225 °C; ^{1}H NMR (500 MHz, DMSO-d_6) δ ppm: 10.10 (s, 1H, NH), 7.93 (d, J = 8.8 Hz, 2H, Ar–H, H-2 & H-6 of –C_6H_5), 7.85 (s, 1H, Ar–H, H-2 of –C_6H_4), 7.83 (d, J = 2.3 Hz, 1H, Ar–H, H-4 of –C_6H_4), 7.76–7.73 (m, 2H, Ar–H, H-5 & H-6 of –C_6H_4), 7.57–7.53 (m, 3H, Ar–H, H-3, H-4 & H-5 of –C_6H_5), 2.53 (s, 3H, $COCH_3$), 2.45 (s, 3H, SCH_3); ^{13}C NMR (126 MHz, DMSO-d_6) δ ppm: 197.26, 174.64, 168.73, 160.40, 142.76, 136.38, 132.96, 131.80, 129.36 (2C), 129.30 (2C), 129.12 (2C),

122.83 (2C), 116.65, 86.16, 27.11, 14.37; molecular formula $C_{20}H_{16}N_4OS$ (360.44).

4.1.2. 4-[(5-Cyano-2-(methylthio)-6-phenylpyrimidin-4-yl) amino]benzoyl chloride 7. To a suspension of compound **4** (3.62 g, 0.01 mol) in dichloromethane (20 mL), thionyl chloride (15 mL) was added and the mixture was heated gently under reflux for 2–3 h. Then, the reaction mixture was filtrated while hot, and the excess of thionyl chloride was removed under vacuum. After cooling, the formed yellow crystals were washed with diethyl ether several times and dried to afford the intermediate compound 7.

4.1.3. 4-[(5-Cyano-2-(methylthio)-6-phenylpyrimidin-4-yl) amino]benzohydrazide 8. Hydrazine hydrate 70% (0.5 mL, 0.5 g, 0.1 mol) was added to a stirred mixture of compound 7 (3.80 g, 0.01 mol) and absolute ethanol (50 mL) in ice bath. The reaction mixture was further stirred for 30–60 min. After completion of reaction, the formed precipitate was filtered. The cropped powder was crystallized from ethanol to afford the target compounds **8**.

White crystals (yield 90%, 3.4 g); mp = 294–295 °C; IR (KBr) ν cm^{-1}: 3296 (NH), 3202 (NH_2), 3035 (CH aromatic), 2922 (CH aliphatic), 2213 (C≡N), 1658 (C=O), 1602 (C=N); ^{1}H NMR (500 MHz, DMSO-d_6) δ ppm: 9.97 (s, 1H, CONH), 9.74 (s, 1H, NH), 7.84 (d, J = 6.6 Hz, 2H, Ar–H, H-3 & H-5 of –C_6H_4), 7.79 (d, J = 8.7 Hz, 2H, Ar–H, H-2 & H-6 of –C_6H_5), 7.67 (d, J = 8.8 Hz, 2H, Ar–H, H-2 & H-6 of –C_6H_4), 7.58–7.53 (m, 3H, Ar–H, H-3, H-4 & H-5 of –C_6H_5), 4.72 (s, 2H, NH_2), 2.44 (s, 3H, SCH_3); ^{13}C NMR (126 MHz, DMSO-d_6) δ ppm: 174.71, 168.71, 165.98, 160.46, 140.92, 136.35, 131.81, 129.62, 129.29 (2C), 129.12 (2C), 127.81 (2C), 123.17 (2C), 116.51, 85.61, 14.32; molecular formula $C_{19}H_{16}N_6OS$ (376.44).

4.1.4. General procedure for synthesis of compounds 9a–d. Equimolar amounts of compound 8 (0.25 g, 0.0067 mol) and the appropriate aldehydes namely, 2-chlorobenzaldehyde, 4-chlorobenzaldehyde, 2,4-dichlorobenzaldehyde, and 2,6-dichlorobenzaldehyde (0.001 mol) were refluxed in absolute ethanol (25 mL) with catalytic amount of glacial acetic acid for 3–6 h. The reaction was followed up by TLC. After completion of reaction, the mixture was cooled. The precipitate formed was filtered, dried and recrystallized from ethanol to give the corresponding compounds **9a–d**, respectively.

*4.1.4.1. N-(2-Chlorobenzylidene)-4-[(5-cyano-2-(methylthio)-6-phenyl pyrimidin-4-yl)-amino]benzohydrazide **9a**.* White fluffy powder (yield 84.5%, 0.27 g); mp = 300–301 °C; IR (KBr) ν cm^{-1}: 3276, 3236 (NH), 3062 (CH aromatic), 2931 (CH aliphatic), 2222 (C≡N), 1649 (C=O), 1599 (C=N); ^{1}H NMR (500 MHz, DMSO-d_6) δ ppm: 12.05 (s, 1H, CONH), 10.08 (s, 1H, NH), 8.84 (s, 1H, N=CH), 8.00 (d, J = 5.6 Hz, 1H, Ar–H, H-6 of 2-ClC_6H_4), 7.93 (d, J = 8.4 Hz, 2H, Ar–H, H-3 & H-5 of –C_6H_4), 7.85 (d, J = 7.5 Hz, 2H, Ar–H, H-2 & H-6 of –C_6H_5), 7.79 (d, J = 8.2 Hz, 2H, Ar–H, H-2 & H-6 of –C_6H_4), 7.60–7.53 (m, 3H, Ar–H, H-3, H-4 & H-5 of –C_6H_5), 7.50 (d, J = 7.5 Hz, 1H, Ar–H, H-3 of 2-Cl–C_6H_4), 7.43–7.39 (m, 2H, Ar–H, H-4 & H-5 of 2-Cl–C_6H_4), 2.48 (s, 3H, SCH_3); ^{13}C NMR (126 MHz, DMSO-d_6) δ ppm: 174.78, 168.76, 163.05, 160.43, 143.89, 141.79, 136.32, 133.71, 132.17, 132.02, 131.85, 130.50, 129.32 (3C), 129.14 (3C), 128.64, 128.20, 127.39, 123.06 (2C), 116.50, 85.80, 14.40; molecular formula $C_{26}H_{19}ClN_6OS$ (498.99).

*4.1.4.2. N-(4-Chlorobenzylidene)-4-[(5-cyano-2-(methylthio)-6-phen-ylpyrimidin-4-yl)-amino]benzohydrazide **9b**.* Off-white fluffy powder (yield 83.9%, 0.275 g); mp = 309–310 °C; HPLC purity 99.53%; IR (KBr) ν cm^{-1}: 3300, 3227 (NH), 3062 (CH aromatic), 2924 (CH aliphatic), 2214 (C≡N), 1650 (C=O), 1607 (C=N); ^{1}H NMR (500 MHz, DMSO-d_6) δ ppm: 11.89 (s, 1H, CONH), 10.07 (s, 1H, NH), 8.41 (s, 1H, N=CH), 7.91 (d, J = 8.4 Hz, 2H, Ar–H, H-3 & H-5 of –C_6H_4), 7.85 (d, 2H, J = 6.8 Hz, Ar–H, H-2 & H-6 of –C_6H_5), 7.77 (d, J = 8.4 Hz, 2H, Ar–H, H-2 & H-6 of –C_6H_4), 7.72 (d, J = 8.3 Hz, 2H, Ar–H, H-2 & H-6 of 4-ClC_6H_4), 7.57–7.49 (m, 3H, Ar–H, H-3, H-4 & H-5 of –C_6H_5), 7.50 (d, J = 8.1 Hz, 2H, Ar–H, H-3 & H-5 of 4-ClC_6H_4), 2.48 (s, 3H, SCH_3); ^{13}C NMR (126 MHz, DMSO-d_6) δ ppm: 174.77, 168.76, 163.06, 160.44, 146.65, 141.70, 136.33, 134.99, 133.88, 131.85, 129.51 (2C), 129.31 (3C), 129.25, 129.14 (3C), 128.59 (2C), 123.09 (2C), 116.52, 85.79, 14.39; MS (m/z): 497.99 (M^+, 31.63%), 500.61 (M^{2+}, 28.55%), 462.04 (100%, base peak); molecular formula $C_{26}H_{19}ClN_6OS$ (498.99).

*4.1.4.3. 4-[(5-Cyano-2-(methylthio)-6-phenylpyrimidin-4-yl) amino]-N-(2,4-dichloro-benzylidene)benzohydrazide **9c**.* Off-white powder (yield 85.6%, 0.30 g); mp = 290–291 °C; HPLC purity 97.46%; IR (KBr) ν cm^{-1}: 3303, 3201 (NH), 3043 (CH aromatic), 2925 (CH aliphatic), 2215 (C≡N), 1650 (C=O), 1612 (C=N); ^{1}H NMR (500 MHz, DMSO-d_6) δ ppm: 12.09 (s, 1H, CONH), 10.07 (s, 1H, NH), 8.78 (s, 1H, N=CH), 7.99 (d, J = 8.5 Hz, 1H, Ar–H, H-6 of –C_6H_3), 7.93 (d, J = 8.5 Hz, 2H, Ar–H, H-3 & H-5 of –C_6H_4), 7.85 (d, J = 7.4 Hz, 2H, Ar–H, H-2 & H-6 of –C_6H_5), 7.79 (d, J = 8.4 Hz, 2H, Ar–H, H-2 & H-6 of –C_6H_4), 7.70 (s, 1H, Ar–H, H-3 of –C_6H_3), 7.60–7.49 (m, 3H, Ar–H, H-3, H-4 & H-5 of –C_6H_5), 7.50 (d, J = 8.6 Hz, 1H, Ar–H, H-5 of –C_6H_3), 2.48 (s, 3H, SCH_3); ^{13}C NMR (126 MHz, DMSO-d_6) δ ppm: 174.78, 168.77, 163.05, 160.43, 142.81, 141.89, 136.32, 135.57, 134.37, 131.86, 131.31, 129.96, 129.32 (3C), 129.14 (3C), 129.03, 128.66, 128.58, 123.07 (2C), 116.51, 85.82, 14.40; molecular formula $C_{26}H_{18}Cl_2N_6OS$ (533.43).

*4.1.4.4. 4-[(5-Cyano-2-(methylthio)-6-phenylpyrimidin-4-yl) amino]-N-(2,6-dichloro-benzylidene)benzohydrazide **9d**.* White fluffy powder (yield 82.8%, 0.29 g); mp = 298–299 °C; IR (KBr) ν cm^{-1}: 3311, 3202 (NH), 3062 (CH aromatic), 2926 (CH aliphatic), 2218 (C≡N), 1645 (C=O), 1610 (C=N); ^{1}H NMR (500 MHz, DMSO-d_6) δ ppm: 12.11 (s, 1H, CONH), 10.07 (s, 1H, NH), 8.62 (s, 1H, N=CH), 7.93 (d, J = 8.5 Hz, 2H, Ar–H, H-3 & H-5 of –C_6H_4), 7.85 (d, J = 7.2 Hz, 2H, Ar–H, H-2 & H-6 of –C_6H_5), 7.78 (d, J = 8.5 Hz, 2H, Ar–H, H-2 & H-6 of –C_6H_4), 7.59–7.54 (m, 5H, Ar–H, H-3 & H-5 of –C_6H_3 and H-3, H4 & H5 of –C_6H_5), 7.42 (t, J = 8.1 Hz, 1H, Ar–H, H-4 of –C_6H_3), 2.50 (s, 3H, SCH_3); ^{13}C NMR (126 MHz, DMSO-d_6) δ ppm: 177.55, 171.12, 165.64, 160.46, 147.49, 136.34, 131.85, 129.67 (4C), 129.31 (5C), 129.14 (4C), 123.09, 115.53, 113.17, 112.36, 81.83, 14.38; molecular formula $C_{26}H_{18}C_{12}N_6OS$ (533.43).

4.1.5. General procedure for synthesis of target compounds 11a–e. To a solution of compound **5** (0.25 g, 0.0069 mol) in absolute ethanol (30 mL), the appropriate benzohydrazide derivatives **10a–e** namely, benzohydrazide, 2-chlorobenzohydrazide, 4-chlorobenzohydrazide, 4-nitrobenzohydrazide, and 2,4-dinitrobenzohydrazide (0.001 mol) were added. The reaction mixture was refluxed with

vigorous stirring till completion of the reaction (4–6 h). After completion of the reaction, the reaction mixture was cooled to room temperature and poured onto ice water (100 mL). The crude product formed was filtered, washed with water, and crystallized from ethanol to afford the corresponding derivatives **11a–e**.

4.1.5.1. N-(1-(4-[(5-Cyano-2-(methylthio)-6-phenylpyrimidin-4-yl)amino]phenyl)ethylidene)benzohydrazide ***11a.*** Off-white powder (yield 90.3%, 0.30 g); mp = 251–252 °C; IR (KBr) ν cm^{-1}: 3294, 3229 (NH), 3055 (CH aromatic), 2921 (CH aliphatic), 2216 (C≡N), 1650 (C═O), 1612 (C═N); ^{1}H NMR (500 MHz, DMSO-d_6) δ ppm: 10.74 (s, 1H, CONH), 9.97 (s, 1H, NH), 7.85–7.82 (m, 4H, Ar–H, H-2 & H-6 of –C_6H_5 and H-2 & H-6 of –COC_6H_5), 7.69 (d, J = 8.1 Hz, 2H, Ar–H, H-2 & H-6 of –C_6H_4), 7.61–7.51 (m, 6H, Ar–H, H-3 & H-5 of –C_6H_4, H-3 & H-5 of –C_6H_5 and H-3 & H-5 of –COC_6H_5), 7.50–7.47 (m, 2H, Ar–H, H-4 of –COC_6H_5 and H-4 of –C_6H_5), 2.46 (s, 3H, SCH_3), 2.34 (s, 3H, CH_3); ^{13}C NMR (126 MHz, DMSO-d_6) δ ppm: 174.71, 168.69, 160.40, 155.46, 139.55, 136.40, 134.65, 131.79, 129.29 (4C), 129.12 (4C), 128.91, 128.43, 127.10, 123.41 (2C), 122.81, 116.58, 111.45, 85.45, 14.94, 14.37; molecular formula $C_{27}H_{22}N_6OS$ (478.57).

4.1.5.2. 2-Chloro-N-(1-(4-[(5-cyano-2-(methylthio)-6-phenylpyrimidin-4-yl)amino]phenyl)-ethylidene)benzohydrazide ***11b.*** Off-white fluffy powder (yield 80%, 0.28 g); mp = 232–233 °C; HPLC purity 99.01%; IR (KBr) ν cm^{-1}: 3300, 3224 (NH), 3057 (CH aromatic), 2924 (CH aliphatic), 2214 (C≡N), 1658 (C═O), 1612 (C═N); ^{1}H NMR (500 MHz, DMSO-d_6) δ ppm: 11.09 (d, J = 125.9 Hz, 1H, CONH), 9.90 (d, J = 67.3 Hz, 1H, NH), 7.85–7.81 (m, 3H, Ar–H, H-2 & H-6 of –C_6H_5 and H-6 of 2-ClC_6H_4), 7.69 (d, J = 8.4 Hz, 1H, Ar–H, H-5 of 2-ClC_6H_4), 7.58–7.51 (m, 4H, Ar–H, H-2, H-3, H-5 & H-6 of –C_6H_4), 7.50–7.45 (m, 2H, Ar–H, H-3 & H-5 of –C_6H_5), 7.43–7.35 (m, 3H, Ar–H, H-4 of –C_6H_4 and H-3 & H-4 of 2-ClC_6H_4), 2.42 (d, J = 32.2 Hz, 3H, SCH_3), 2.26 (d, J = 16.6 Hz, 3H, CH_3); ^{13}C NMR (126 MHz, DMSO-d_6) δ ppm: 174.73–174.61, 170.13, 168.69–168.62, 163.53, 160.40–160.33, 154.52, 148.58, 139.59, 139.03, 137.29, 136.38, 136.31, 134.69, 134.50, 131.77, 131.67, 131.01, 130.81, 130.24, 130.11, 129.35, 129.28, 129.10 (2C), 127.68, 127.38, 127.12, 126.40, 123.37, 116.54, 85.46, 85.37, 14.96, 14.39, 14.2, 14.15; molecular formula $C_{27}H_{21}ClN_6OS$ (513.02).

4.1.5.3. 3-Chloro-N-(1-(4-[(5-cyano-2-(methylthio)-6-phenylpyramid-in-4-yl)amino]-phenyl)ethylidene)benzohydrazide ***11c.*** Yellow powder (yield 80.1%, 0.285 g); mp = 262–263 °C; HPLC purity 96.25%; IR (KBr) ν cm^{-1}: 3306, 3194 (NH), 3060 (CH aromatic), 2926 (CH aliphatic), 2222 (C≡N), 1666 (C═O), 1620 (C═N); ^{1}H NMR (400 MHz, DMSO-d_6) δ ppm: 10.88 (s, 1H, CONH), 9.98 (s, 1H, NH), 7.96–7.86 (m, 5H, Ar–H, H-2 & H-6 of –C_6H_5 and H-2, H-4 & H-6 of 3-ClC_6H_4), 7.74 (d, J = 9.1 Hz, 2H, Ar–H, H-2 & H-6 of –C_6H_4), 7.67 (d, J = 9.9 Hz, 2H, Ar–H, H-3 & H-5 of –C_6H_4), 7.63–7.57 (m, 4H, Ar–H, H-3, H-4 & H-5 of –C_6H_5 and H-5 of 3-ClC_6H_4), 2.51 (s, 3H, SCH_3), 2.40 (s, 3H, –CH_3); ^{13}C NMR (101 MHz, DMSO-d_6) δ ppm: 174.66, 168.61, 163.03, 160.36, 136.35, 134.48, 131.71, 131.07, 129.21 (4C), 129.04 (4C), 128.08, 127.12, 125.52, 123.31 (3C), 116.46, 85.45, 56.51, 19.02, 14.30; MS (m/z): 513.59 (M^+, 14.25%), 515.73 (M^+ + 2, 10.12%), 172.61 (100%, base peak); molecular formula $C_{27}H_{21}ClN_6OS$ (513.02).

4.1.5.4. N-(1-(4-[(5-Cyano-2-(methylthio)-6-phenylpyrimidin-4-yl)amino]phenyl)-ethylidene)-4-nitrobenzohydrazide ***11d.*** Yellow fluffy powder (yield 78.5%, 0.285 g); mp = 268–269 °C; HPLC purity 93.41%; IR (KBr) ν cm^{-1}: 3307, 3210 (NH), 3007 (CH aromatic), 2924 (CH aliphatic), 2213 (C≡N), 1657 (C═O), 1611 (C═N), 1528, 1343 (NO_2); ^{1}H NMR (500 MHz, DMSO-d_6) δ ppm: 11.06 (s, 1H, CONH), 9.98 (s, 1H, NH), 8.32 (d, J = 8.4 Hz, 2H, Ar–H, H-3 & H-5 of 4-$NO_2C_6H_4$), 8.09 (d, J = 8.7 Hz, 2H, Ar–H, H-2 & H-6 of 4-$NO_2C_6H_4$), 7.87 (d, J = 8.5 Hz, 2H, Ar–H, H-2 & H-6 of –C_6H_4), 7.84 (d, J = 7.1 Hz, 2H, Ar–H, H-2 & H-6 of –C_6H_5), 7.70 (d, J = 8.2 Hz, 2H, Ar–H, H-3 & H-5 of –C_6H_4), 7.58–7.54 (m, 3H, Ar–H, H-3, H-4 & H-5 of –C_6H_5), 2.46 (s, 3H, SCH_3), 2.36 (s, 3H, CH_3); ^{13}C NMR (126 MHz, DMSO-d_6) δ ppm: 174.72, 168.68, 162.95, 160.39, 156.81, 149.62, 140.43, 139.82, 136.38, 134.33, 131.79, 131.13, 129.99, 129.36, 129.29 (2C), 129.11 (2C), 127.23, 126.73, 124.02, 123.37, 122.80, 116.56, 85.49, 15.19, 14.38; molecular formula $C_{27}H_{21}N_7O_3S$ (523.57).

4.1.5.5. N-(1-(4-[(5-Cyano-2-(methylthio)-6-phenylpyrimidin-4-yl)amino]phenyl)-ethylidene)-2,4-dinitrobenzohydrazide ***11e.*** Reddish-orange fine powder (yield 67.1%, 0.265 g); mp = 298–299 °C; IR (KBr) ν cm^{-1}: 3297, 3204 (NH), 3113 (CH aromatic), 2925 (CH aliphatic), 2209 (C≡N), 1614 (C═N), 1550, 1362 (NO_2); ^{1}H NMR (500 MHz, DMSO-d_6) δ ppm: 11.11 (s, 1H, CONH), 10.01 (s, 1H, NH), 8.87 (d, J = 3.1 Hz, 1H, Ar–H, H-3 of –C_6H_3), 8.38 (dd, J = 9.6, 2.5 Hz, 1H, Ar–H, H-5 of –C_6H_3), 8.11 (d, J = 9.6 Hz, 1H, Ar–H, H-6 of –C_6H_3), 7.96 (d, J = 8.8 Hz, 2H, Ar–H, H-2 & H-6 of –C_6H_4), 7.85 (d, J = 6.9 Hz, 2H, Ar–H, H-2 & H-6 of –C_6H_5), 7.74 (d, J = 8.7 Hz, 2H, Ar–H, H-3 & H-5 of –C_6H_4), 7.60–7.54 (m, 3H, Ar–H, H-3, H-4 & H-5 of –C_6H_5), 2.48 (s, 3H, SCH_3), 2.44 (s, 3H, CH_3); ^{13}C NMR (126 MHz, DMSO-d_6) δ ppm: 174.74, 168.71, 166.67, 160.35, 146.91, 144.96, 142.13, 140.07, 136.38, 133.43, 131.53, 130.72, 130.16, 129.31 (2C), 129.14 (2C), 127.28 (2C), 124.09, 123.40 (2C), 117.17, 116.13, 86.39, 14.41, 13.77; molecular formula $C_{27}H_{20}N_8O_5S$ (568.57).

4.1.6. General procedure for synthesis of target compounds 12a–g. To a solution of compound 6 (0.25 g, 0.0069 mol) in absolute ethanol (30 mL), the appropriate benzohydrazide derivatives 10a-h namely, benzohydrazide, 2-chlorobenzohydrazide, 3-chlorobenzohydrazide, 4-nitrobenzohydrazide, 2-hydroxybenzohydrazide, 4-hydroxybenzo- hydrazide, and 4-aminobenzohydrazide (0.001 mol) were added. The mixture was heated at refluxing temperature for 4–6 h. After completion of the reaction, the reaction mixture was cooled to room temperature and poured onto ice water (100 mL). The crude product formed was filtered, washed with water, and crystallized from ethanol to afford the corresponding derivatives **12a–g**, respectively.

4.1.6.1. N-(1-(3-[(5-Cyano-2-(methylthio)-6-phenylpyrimidin-4-yl)amino]phenyl)-ethylidene)benzohydrazide ***12a.*** Beige fluffy powder (yield 87.3%, 0.29 g); mp = 242–225 °C; HPLC purity 99.38%; IR (KBr) ν cm^{-1}: 3341, 3254 (NH), 3056 (CH aromatic), 2926 (CH aliphatic), 2206 (C≡N), 1649 (C═O), 1615 (C═N); ^{1}H NMR (400 MHz, DMSO-d_6) δ ppm: 10.80 (s, 1H, CONH), 9.98 (s, 1H, NH), 7.92–7.87 (m, 4H, Ar–H, H-2, H-6 of –C_6H_5 and Ar–H, H-2 & H-6 of –COC_6H_5), 7.70–7.67 (m, 2H, Ar–H, H-4 of –C_6H_4 and H-4 –COC_6H_5), 7.62–7.59 (m, 5H, Ar–H, H-3, H-4, H-5 of –

C_6H_5 and H-3 & H-5 of $-COC_6H_4$), 7.54 (d, J = 7.3 Hz, 2H, Ar–H, H-2 & H-5 of $-C_6H_4$), 7.47 (d, J = 8.00 Hz, 1H, Ar–H, H-6 of $-C_6H_4$), 2.47 (s, 3H, SCH_3), 2.40 (s, 3H, CH_3); ^{13}C NMR (101 MHz, DMSO-d_6) δ ppm: 174.63, 168.58, 161.83, 160.58, 155.46, 138.85, 138.33, 136.40, 134.55, 132.02, 131.65, 129.19 (3C), 129.03 (3C), 128.83 (2C), 128.42, 125.10, 123.44, 122.10, 116.49, 85.10, 15.03, 14.22; molecular formula $C_{27}H_{22}N_6OS$ (478.57).

4.1.6.2. 2-Chloro-N-(1-(3-[(5-cyano-2-(methylthio)-6-phenyl pyri-midin-4-yl)amino]-phenyl)ethylidene)benzohydrazide ***12b***. White fluffy powder (yield 77%, 0.27 g); mp = 221–222 °C; IR (KBr) ν cm^{-1}: 3396 (NH), 3147, 3026 (CH aromatic), 2993 (CH aliphatic), 2202 (C≡N), 1664 (C=O), 1613 (C=N); ^{1}H NMR (500 MHz, DMSO-d_6) δ ppm: 11.13 (d, J = 136.2 Hz, 1H, CONH), 9.96 (d, J = 72.0 Hz, 1H, NH), 8.17 (d, J = 34.5 Hz, 1H, Ar–H, H-2 of $-C_6H_4$), 7.84 (d, J = 7.2 Hz, 2H, Ar–H, H-2 & H-6 of $-C_6H_5$), 7.69–7.64 (m, 1H, Ar–H, H-6 of $-C_6H_4$), 7.60 (dd, J = 15.0, 7.2 Hz, 1H, Ar–H, H-6 of $-C_6H_4$), 7.56–7.47 (m, J = 12.8, 5.9 Hz, 3H, Ar–H, H-3 of 3-ClC_6H_4 and Ar–H, H-3 & H-5 of $-C_6H_5$), 7.46–7.37 (m, 3H, Ar–H, H-4 of $-C_6H_4$, 4 H-4 of 3-ClC_6H_4 & Ar–H, H-4 of $-C_6H_5$), 7.35–7.27 (m, 1H, Ar–H, H-5 of $-C_6H_4$), 7.25–7.15 (m, 1H, Ar–H, H-5 of 3-ClC_6H_4), 2.45 (s, 3H, SCH_3), 2.27 (s, 3H, CH_3); ^{13}C NMR (126 MHz, DMSO-d_6) δ ppm: 174.70, 170.21, 168.66, 163.60, 160.61, 154.48, 148.32, 138.76, 138.59, 137.14, 136.44, 131.73, 130.99, 130.19, 129.27, 129.10, 128.90, 127.69, 125.22, 24.86, 123.58, 122.53, 116.58, 85.16, 84.92, 15.38, 14.30; molecular formula $C_{27}H_{21}ClN_6OS$ (513.02).

4.1.6.3. 3-Chloro-N-(1-(3-[(5-cyano-2-(methylthio)-6-phenylpyramidin-4-yl)amino]phenyl)-ethylidene)benzohydrazide ***12c***. Beige crystals (yield 87%, 0.31 g); mp = 230–231 °C; HPLC purity 100%; IR (KBr) ν cm^{-1}: 3308, 3178 (NH), 3067 (CH aromatic), 2923 (CH aliphatic), 2216 (C≡N), 1669 (C=O), 1628 (C=N); ^{1}H NMR (400 MHz, DMSO-d_6) δ ppm: 10.91 (s, 1H, CONH), 10.00 (s, 1H, NH), 8.18 (s, 1H, Ar–H, H-2 of 3-ClC_6H_4), 7.96 (s, 1H, Ar–H, H-6 of 3-ClC_6H_4), 7.90–7.88 (m, 3H, Ar–H, H-4 of $-C_6H_4$ and H-2 & H-6 of $-C_6H_5$), 7.63–7.53 (m, 6H, Ar–H, H-2 of $-C_6H_4$, H-4, H-5 of 3-ClC_6H_4 and Ar–H, H-3, H-4 & H-5 of $-C_6H_5$), 7.57–7.53 (m, 1H, Ar–H, H-5 of $-C_6H_4$), 7.46 (d, J = 4.00 Hz, 1H, Ar–H, H-6 of $-C_6H_4$), 2.47 (s, 3H, SCH_3), 2.41 (s, 3H, CH_3); ^{13}C NMR (101 MHz, DMSO-d_6) δ ppm: 174.62, 168.56, 162.95, 160.60, 150.58, 138.71, 138.37, 137.74, 136.42, 136.35, 133.22, 131.65, 131.07, 129.17 (2C), 129.02 (2C), 128.86, 128.47, 126.99, 125.04, 123.39, 122.13, 116.47, 85.11, 27.23, 14.20; molecular formula $C_{27}H_{21}ClN_6OS$ (513.02).

4.1.6.4. N-(1-(3-[(5-cyano-2-(methylthio)-6-phenylpyrimidin-4-yl)amino]phenyl)-ethylidene)-4-nitrobenzohydrazide ***12d***. Off-white crystals (yield 80%, 0.29 g); mp = 265–266 °C; IR (KBr) ν cm^{-1}: 3305, 3196 (NH), 3076 (CH aromatic), 2927 (CH aliphatic), 2213 (C≡N), 1670 (C=O), 1597 (C=N), 1543, 1345 (NO_2); ^{1}H NMR (400 MHz, DMSO-d_6) δ ppm: 11.10 (s, 1H, CONH), 9.98 (s, 1H, NH), 8.36 (d, J = 8.0 Hz, 2H, Ar–H, H-3 & H-5 of 4-$NO_2C_6H_4$), 8.16 (d, 2H, Ar–H, H-2 & H-6 of 4-$NO_2C_6H_4$), 8.06 (s, 1H, Ar–H, H-2 of $-C_6H_4$), 7.89 (d, 2H, J = 8.0 Hz, Ar–H, H-2 & H-6 of $-C_6H_5$), 7.71–7.68 (m, 1H, Ar–H, H-5 of $-C_6H_4$), 7.61–7.59 (m, 4H, Ar–H, H-3, H-4 & H-5 of $-C_6H_5$ and H-4 of $-C_6H_4$), 7.47 (d, 1H, Ar–H, H-6 of $-C_6H_4$), 2.51 (s, 3H, SCH_3), 2.20 (s, 3H, CH_3); ^{13}C NMR (101 MHz, DMSO-d_6) δ ppm: 174.61, 168.58, 164.39, 163.07, 160.56, 138.15, 137.19, 136.39, 131.65, 129.95 (3C), 129.19 (2C), 129.05 (2C), 129.01, 128.92, 125.36, 124.02, 123.93, 123.70, 122.14, 116.50, 85.11, 15.04, 14.21; molecular formula $C_{27}H_{21}N_7O_3S$ (523.57).

4.1.6.5. N-(1-(3-[(5-Cyano-2-(methylthio)-6-phenylpyrimidin-4-yl)amino]phenyl)-ethylidene)-2-hydroxybenzohydrazide ***12e***. Beige crystals (yield 79%, 0.27 g); mp = 204–205 °C; IR (KBr) ν cm^{-1}: 3392 (OH), 3297 (NH), 3060 (CH aromatic), 2925 (CH aliphatic), 2213 (C≡N), 1649 (C=O), 1602 (C=N); ^{1}H NMR (500 MHz, DMSO-d_6) δ ppm: 11.39 (s, 1H, OH), 9.97 (s, 1H, CONH), 8.14 (s, 1H, NH), 7.96 (d, J = 5.00 Hz, 1H, Ar–H, H-6 of 2-OHC_6H_4), 7.84 (d, J = 7.2 Hz, 2H, Ar–H, H-2 & H-6 of $-C_6H_5$), 7.66–7.61 (m, 2H, Ar–H, H-5 of $-C_6H_4$ & H-4 of 2-OHC_6H_4), 7.60–7.51 (m, 4H, Ar–H, H-3, H-4 & H-5 of $-C_6H_5$ and H-4 of $-C_6H_4$), 7.43–7.37 (m, 2H, Ar–H, H-2 & H-6 of $-C_6H_4$), 6.99 (d, J = 8.2 Hz, 1H, Ar–H, H-3 of 2-OHC_6H_4), 6.94 (t, J = 7.6 Hz, 1H, Ar–H, H-5 of 2-OHC_6H_4), 2.43 (s, 3H, SCH_3), 2.32 (s, 3H, CH_3); ^{13}C NMR (126 MHz, DMSO-d_6) δ ppm: 174.71, 168.65, 162.55, 160.62, 157.21, 152.12, 138.69, 138.39, 136.45, 133.94, 131.73, 131.21, 129.27 (2C), 129.10 (2C), 128.93, 125.11, 123.56, 122.04, 120.13, 118.44, 117.47, 116.58, 85.13, 14.42, 14.30; molecular formula $C_{27}H_{22}N_6O_2S$ (494.57).

4.1.6.6. N-(1-(3-[(5-Cyano-2-(methylthio)-6-phenylpyrimidin-4-yl)amino]phenyl)-ethylidene)-4-hydroxybenzohydrazide ***12f***. Beige fine powder (yield 75.8%, 0.26 g); mp = 231–232 °C; HPLC purity 94.88%; IR (KBr) ν cm^{-1}: 3316 (OH), 3270, 3196 (NH), 3011 (CH aromatic), 2806 (CH aliphatic), 2204 (C≡N), 1659 (C=O), 1614 (C=N); ^{1}H NMR (400 MHz, DMSO-d_6) δ ppm: 10.53 (s, 1H, CONH), 9.99 (s, 1H, OH), 9.49 (s, 1H, NH), 7.89 (d, J = 7.5 Hz, 2H, Ar–H, H-2 & H-6 of $-C_6H_5$), 7.81 (d, J = 8.3 Hz, 1H, Ar–H, H-4 of $-C_6H_4$), 7.71–7.67 (m, 3H, Ar–H, H-2 & H-6 of 4-OHC_6H_4 and H-2 of $-C_6H_4$), 7.64–7.59 (m, 3H, Ar–H, H-3, H-4 & H-5 of $-C_6H_5$), 7.45 (t, J = 8.0 Hz, 1H, Ar–H, H-5 of $-C_6H_4$), 6.87 (d, J = 8.4 Hz, 1H, Ar–H, H-6 of $-C_6H_4$), 6.79 (d, J = 8.2 Hz, 2H, Ar–H, H-3 & H-5 of 4-OHC_6H_4), 2.47 (s, 3H, SCH_3), 2.38 (s, 3H, CH_3); ^{13}C NMR (101 MHz, DMSO-d_6) δ ppm: 174.61, 168.57, 166.40, 161.01, 160.57, 160.47, 139.00, 136.42, 131.64, 129.28 (3C), 129.19 (2C), 129.02 (2C), 128.80, 124.90, 124.44, 123.34, 122.03, 115.29 (3C), 85.10, 14.80, 14.21; MS (m/z): 494.37 (M^+, 54.40%), 419.31 (100%, base peak); molecular formula $C_{27}H_{22}N_6O_2S$ (494.57).

4.1.6.7. 4-Amino-N-(1-(3-[(5-cyano-2-(methylthio)-6-phenylpyrimidin-4-yl)amino]phenyl)-ethylidene)benzohydrazide ***12g***. White fluffy powder (yield 80%, 0.27 g); mp = 227–228 °C; IR (KBr) ν cm^{-1}: 3478, 3363, 3293 (2NH, NH_2), 3071 (CH aromatic), 2924, (CH aliphatic), 2215 (C≡N), 1637 (C=O), 1606 (C=N); ^{1}H NMR (400 MHz, DMSO-d_6) δ ppm: 10.29 (s, 1H, CONH), 9.97 (s, 1H, NH), 8.12 (s, 1H, Ar–H, H-4 of $-C_6H_4$), 7.91 (d, J = 8.00 Hz, 2H, Ar–H, H-2 & H-6 of $-C_6H_5$), 7.68 (d, J = 8.4 Hz, 2H, Ar–H, H-2 & H-6 of 4-$NH_2C_6H_4$), 7.65 (d, J = 3.9 Hz, 1H, Ar–H, H-6 of $-C_6H_4$), 7.64–7.56 (m, 4H, Ar–H, H-2 of $-C_6H_4$, and H-3, H-4 & H-5 of $-C_6H_5$), 7.45 (t, J = 7.9 Hz, 1H, Ar–H, H-5 of $-C_6H_4$), 6.61 (d, J = 8.3 Hz, 2H, Ar–H, H-3 & H-5 of 4-$NH_2C_6H_4$), 5.75 (s, 2H, NH_2), 2.47 (s, 3H, SCH_3), 2.37 (s, 3H, CH_3); ^{13}C NMR (101 MHz, DMSO-d_6) δ ppm: 174.61, 168.57, 164.59, 160.57, 152.66, 139.18, 138.35, 136.43, 131.63, 130.31, 129.19 (3C), 129.02 (3C), 128.76, 124.79, 123.26, 121.97, 120.53, 116.52, 113.00 (2C), 85.09, 14.60, 14.22; molecular formula $C_{27}H_{23}N_7OS$ (493.59).

4.2. Biological evaluation

4.2.1. *In vitro* antiproliferative activities. The *in vitro* antiproliferative activeness of all the synthesized derivatives had been evaluated towards HCT-116 and MCF-7 cell lines, using the MTT assay protocol[25–27] as prescribed in as shown in ESI.† Sorafenib was utilized as the reference drug.

The cell lines were obtained from the Holding company for biological products and vaccines (VACSERA), Cairo, Egypt.

4.2.2. *In vitro* cytotoxicity against normal human lung cells. Cytotoxic activity of the most active anti-proliferative compound **11e** was estimated against normal human lung cells (WI-38) using the MTT assay protocol[41] as shown in ESI.†

4.2.3. *In vitro* VEGFR-2 kinase inhibitory assay. The VEGFR-2 inhibitory activity for the most active cytotoxic compounds (**9d**, **11b**, **11c**, **11d**, **11e**, **12b**, **12c**, and **12d**) were assessed *in vitro* using the Human VEGFR-2 TK ELISA kit as shown in ESI.†

4.2.4. *In vitro* DNA-flow cytometric (cell cycle) analysis. To investigate the effect of compound **11e** on the various phases of the cell cycle, flow cytometric analysis of cell cycle was performed using Epics XL-MCL™ Flow Cytometer[22,41] as shown in ESI.†

4.2.5. Annexin V-FITC apoptosis assay. Apoptotic effect of compound **11e** on the treated cells was analyzed with the aid of Annexin V-FITC-apoptosis detection kit (PN IM3546) using Epics XL-MCL™ Flow Cytometer[33,41] as prescribed in ESI.†

4.2.6. *In vitro* immunomodulatory assay of TNF-α and IL-6. Cell culture supernatants as well as cell lysate were prepared from HepG2 cancer cell line utilized for immunoassay using different kits.[24,42,43] The protocols for cell culture supernatants and cell lysate preparation were written in details in ESI.†

4.2.7. Assessment of caspase-3 expression. The levels of caspase-3, cell culture supernatants was estimated by ELISA technique using commercially available matched paired antibodies (R&D Systems Inc., Minneapolis, MN) according to reported procedure[44] and described in details in ESI.†

4.3. *In silico* studies

4.3.1. Docking studies. Docking studies towards VEGFR-2 TK (PDB ID 1YWN, resolution: 1.71 Å) were performed by MOE2019 software as shown in ESI.†

4.3.2. MD simulations. MD simulation studies were directed by the CHARMM-GUI web server and GROMACS 2021 as an MD engine as shown in ESI.†[45,46]

4.3.3. MM-GBSA. MM-GBSA and PLIP analyses were performed by the Gmx_MMPBSA package as shown in ESI.†[47]

Conflicts of interest

This work was funded by the authors and there is no any conflict of interest.

Acknowledgements

This paper is based upon work supported by Science, Technology & Innovation Funding Authority (STIFA) under grant number 44434.

References

1 V. Ganapathy, M. Thangaraju and P. D. Prasad, Nutrient transporters in cancer: relevance to Warburg hypothesis and beyond, *Pharmacol. Therapeut.*, 2009, **121**(1), 29–40.
2 H. Varmus, The new era in cancer research, *Science*, 2006, **312**(5777), 1162–1165.
3 Z. Wang, X.-H. Shi, J. Wang, T. Zhou, Y.-Z. Xu, T.-T. Huang, *et al.*, Synthesis, structure–activity relationships and preliminary antitumor evaluation of benzothiazole-2-thiol derivatives as novel apoptosis inducers, *Bioorg. Med. Chem. Lett.*, 2011, **21**(4), 1097–1101.
4 R. L. Siegel, K. D. Miller and A. Jemal, Cancer statistics, *Ca-Cancer J. Clin.*, 2018, **68**(1), 7–30.
5 N. M. Saleh, A. A. H. Abdel-Rahman, A. M. Omar, M. M. Khalifa and K. El-Adl, Pyridine-derived VEGFR-2 inhibitors: rational design, synthesis, anticancer evaluations, in silico ADMET profile, and molecular docking, *Arch. Pharm.*, 2021, **354**(8), 2100085.
6 R. G. Yousef, W. M. Eldehna, A. Elwan, A. S. Abdelaziz, A. B. Mehany, I. M. Gobaara, *et al.*, Design, Synthesis, In Silico and In Vitro Studies of New Immunomodulatory Anticancer Nicotinamide Derivatives Targeting VEGFR-2, *Molecules*, 2022, **27**(13), 4079.
7 F. Ran, W. Li, Y. Qin, T. Yu, Z. Liu, M. Zhou, *et al.*, Inhibition of vascular smooth muscle and cancer cell proliferation by new VEGFR inhibitors and their immunomodulator effect: design, synthesis, and biological evaluation, *Oxid. Med. Cell. Longev.*, 2021, **2021**, 1–21.
8 R. G. Yousef, A. Ibrahim, M. M. Khalifa, W. M. Eldehna, I. M. Gobaara, A. B. Mehany, *et al.*, Discovery of new nicotinamides as apoptotic VEGFR-2 inhibitors: virtual screening, synthesis, anti-proliferative, immunomodulatory, ADMET, toxicity, and molecular dynamic simulation studies, *J. Enzym. Inhib. Med. Chem.*, 2022, **37**(1), 1389–1403.
9 M. S. Taghour, H. A. Mahdy, M. H. Gomaa, A. Aglan, M. G. Eldeib, A. Elwan, *et al.*, Benzoxazole derivatives as new VEGFR-2 inhibitors and apoptosis inducers: design, synthesis, in silico studies, and antiproliferative evaluation, *J. Enzym. Inhib. Med. Chem.*, 2022, **37**(1), 2063–2077.
10 E. B. Elkaeed, R. G. Yousef, M. M. Khalifa, A. Ibrahim, A. B. Mehany, I. M. Gobaara, *et al.*, Discovery of New VEGFR-2 Inhibitors: Design, Synthesis, Anti-Proliferative Evaluation, Docking, and MD Simulation Studies, *Molecules*, 2022, **27**(19), 6203.
11 M. S. Taghour, H. Elkady, W. M. Eldehna, N. M. El-Deeb, A. M. Kenawy, E. B. Elkaeed, *et al.*, Design and synthesis of thiazolidine-2, 4-diones hybrids with 1, 2-dihydroquinolones and 2-oxindoles as potential VEGFR-2 inhibitors: in vitro anticancer evaluation and in silico studies, *J. Enzyme Inhib. Med. Chem.*, 2022, **37**(1), 1903–1917.
12 M. M. Alanazi, H. Elkady, N. A. Alsaif, A. J. Obaidullah, H. M. Alkahtani, M. M. Alanazi, *et al.*, New quinoxaline-based VEGFR-2 inhibitors: design, synthesis, and antiproliferative evaluation with in silico docking, ADMET,

toxicity, and DFT studies, *RSC Adv.*, 2021, **11**(48), 30315–30328.

13 A. R. Kotb, D. A. Bakhotmah, A. E. Abdallah, H. Elkady, M. S. Taghour, I. H. Eissa, *et al.*, Design, synthesis, and biological evaluation of novel bioactive thalidomide analogs as anticancer immunomodulatory agents, *RSC Adv.*, 2022, **12**(52), 33525–33539.

14 I. H. Eissa, M. A. Dahab, M. K. Ibrahim, N. A. Alsaif, A. Alanazi, S. I. Eissa, *et al.*, Design and discovery of new antiproliferative 1, 2, 4-triazin-3 (2H)-ones as tubulin polymerization inhibitors targeting colchicine binding site, *Bioorg. Chem.*, 2021, **112**, 104965.

15 M. A. Abdelgawad, K. El-Adl, S. S. El-Hddad, M. M. Elhady, N. M. Saleh, M. M. Khalifa, *et al.*, Design, molecular docking, synthesis, anticancer and anti-hyperglycemic assessments of thiazolidine-2, 4-diones bearing sulfonylthiourea moieties as potent VEGFR-2 inhibitors and PPARγ agonists, *Pharmaceuticals*, 2022, **15**(2), 226.

16 I. H. Eissa, R. El-Haggar, M. A. Dahab, M. F. Ahmed, H. A. Mahdy, R. I. Alsantali, *et al.*, Design, synthesis, molecular modeling and biological evaluation of novel benzoxazole-benzamide conjugates via a 2-thioacetamido linker as potential anti-proliferative agents, VEGFR-2 inhibitors and apoptotic inducers, *J. Enzyme Inhib. Med. Chem.*, 2022, **37**(1), 1587–1599.

17 M. A. Dahab, H. A. Mahdy, H. Elkady, M. S. Taghour, A. Elwan, M. A. Elkady, *et al.*, Semi-synthesized anticancer theobromine derivatives targeting VEGFR-2: in silico and in vitro evaluations, *J. Biomol. Struct. Dyn.*, 2023, 1–20.

18 N. A. Alsaif, H. A. Mahdy, M. M. Alanazi, A. J. Obaidullah, H. M. Alkahtani, A. M. Al-Hossaini, *et al.*, Targeting VEGFR-2 by new quinoxaline derivatives: design, synthesis, antiproliferative assay, apoptosis induction, and in silico studies, *Arch. Pharm.*, 2022, **355**(2), 2100359.

19 N. A. Alsaif, A. Elwan, M. M. Alanazi, A. J. Obaidullah, W. A. Alanazi, A. F. Alasmari, *et al.*, Design, synthesis and molecular docking of new [1, 2, 4] triazolo [4, 3-a] quinoxaline derivatives as anticancer agents targeting VEGFR-2 kinase, *Mol. Diversity*, 2022, **26**(4), 1915–1932.

20 H. A. Mahdy, M. K. Ibrahim, A. M. Metwaly, A. Belal, A. B. Mehany, K. M. El-Gamal, *et al.*, Design, synthesis, molecular modeling, in vivo studies and anticancer evaluation of quinazolin-4 (3H)-one derivatives as potential VEGFR-2 inhibitors and apoptosis inducers, *Bioorg. Chem.*, 2020, **94**, 103422.

21 S. Kambe, A one step synthesis of 4-oxo-2-thioxopyrimidine derivatives by the ternary condensation of ethyl cyanoacetate, aldehydes, and thiourea, *Synthesis*, 1979, **4**, 287–289.

22 A. A. Nasser, I. H. Eissa, M. R. Oun, M. A. El-Zahabi, M. S. Taghour, A. Belal, *et al.*, Discovery of new pyrimidine-5-carbonitrile derivatives as anticancer agents targeting EGFR WT and EGFR T790M, *Org. Biomol. Chem.*, 2020, **18**(38), 7608–7634.

23 I. A. Osman, R. R. Ayyad and H. A. Mahdy, New pyrimidine-5-carbonitrile derivatives as EGFR inhibitors with anticancer and apoptotic activities: design, molecular modeling and synthesis, *New J. Chem.*, 2022, **46**(24), 11812–11827.

24 M. A. El-Zahabi, H. Sakr, K. El-Adl, M. Zayed, A. S. Abdelraheem, S. I. Eissa, *et al.*, Design, synthesis, and biological evaluation of new challenging thalidomide analogs as potential anticancer immunomodulatory agents, *Bioorg. Chem.*, 2020, **104**, 104218.

25 T. Mosmann, Rapid colorimetric assay for cellular growth and survival: application to proliferation and cytotoxicity assays, *J. Immunol. Methods*, 1983, **65**(1–2), 55–63.

26 F. Denizot and R. Lang, Rapid colorimetric assay for cell growth and survival: modifications to the tetrazolium dye procedure giving improved sensitivity and reliability, *J. Immunol. Methods*, 1986, **89**(2), 271–277.

27 M. Thabrew, R. D. Hughes and I. G. McFarlane, Screening of hepatoprotective plant components using a HepG2 cell cytotoxicity assay, *J. Pharm. Pharmacol.*, 1997, **49**(11), 1132–1135.

28 T. Aiebchun, P. Mahalapbutr, A. Auepattanapong, O. Khaikate, S. Seetaha, L. Tabtimmai, *et al.*, Identification of vinyl sulfone derivatives as egfr tyrosine kinase inhibitor: in vitro and in silico studies, *Molecules*, 2021, **26**(8), 2211.

29 E. M. Mohi El-Deen, M. M. Anwar, A. A. A. El-Gwaad, E. A. Karam, M. K. El-Ashrey and R. R. Kassab, Novel Pyridothienopyrimidine Derivatives: Design, Synthesis and Biological Evaluation as Antimicrobial and Anticancer Agents, *Molecules*, 2022, **27**(3), 803.

30 N. A. Alsaif, A. Elwan, M. M. Alanazi, A. J. Obaidullah, W. A. Alanazi, A. F. Alasmari, *et al.*, Design, synthesis and molecular docking of new [1, 2, 4] triazolo [4, 3-a] quinoxaline derivatives as anticancer agents targeting VEGFR-2 kinase, *Mol. Diversity*, 2021, 1–18.

31 H. Van De Waterbeemd and E. Gifford, ADMET in silico modelling: towards prediction paradise?, *Nat. Rev. Drug Discov.*, 2003, **2**(3), 192–204.

32 A. Elwan, A. E. Abdallah, H. A. Mahdy, M. A. Dahab, M. S. Taghour, E. B. Elkaeed, *et al.*, Modified benzoxazole-based VEGFR-2 inhibitors and apoptosis inducers: design, synthesis, and anti-proliferative evaluation, *Molecules*, 2022, **27**(15), 5047.

33 T. Al-Warhi, M. F. Abo-Ashour, H. Almahli, O. J. Alotaibi, M. M. Al-Sanea, G. H. Al-Ansary, *et al.*, Novel [(N-alkyl-3-indolylmethylene) hydrazono] oxindoles arrest cell cycle and induce cell apoptosis by inhibiting CDK2 and Bcl-2: synthesis, biological evaluation and in silico studies, *J. Enzym. Inhib. Med. Chem.*, 2020, **35**(1), 1300–1309.

34 A. E. Abdallah, I. H. Eissa, A. B. Mehany, H. Sakr, A. Atwa, K. El-Adl, *et al.*, Immunomodulatory quinazoline-based thalidomide analogs: design, synthesis, apoptosis and anticancer evaluations, *J. Mol. Struct.*, 2023, **1281**, 135164.

35 Y. Miyazaki, S. Matsunaga, J. Tang, Y. Maeda, M. Nakano, R. J. Philippe, *et al.*, Novel 4-amino-furo [2, 3-d] pyrimidines as Tie-2 and VEGFR2 dual inhibitors, *Bioorg. Med. Chem. Lett.*, 2005, **15**(9), 2203–2207.

36 M. Hagras, M. A. Saleh, R. R. Ezz Eldin, A. A. Abuelkhir, E. G. Khidr, A. A. El-Husseiny, *et al.*, 1, 3, 4-Oxadiazole-

naphthalene hybrids as potential VEGFR-2 inhibitors: design, synthesis, antiproliferative activity, apoptotic effect, and in silico studies, *J. Enzym. Inhib. Med. Chem.*, 2022, **37**(1), 386–402.

37 A. M. Farghaly, O. M. AboulWafa, Y. A. Elshaier, W. A. Badawi, H. H. Haridy and H. A. Mubarak, Design, synthesis, and antihypertensive activity of new pyrimidine derivatives endowing new pharmacophores, *Med. Chem. Res.*, 2019, **28**, 360–379.

38 N. A. Alsaif, M. A. Dahab, M. M. Alanazi, A. J. Obaidullah, A. A. Al-Mehizia, M. M. Alanazi, *et al.*, New quinoxaline derivatives as VEGFR-2 inhibitors with anticancer and apoptotic activity: Design, molecular modeling, and synthesis, *Bioorg. Chem.*, 2021, **110**, 104807.

39 I. H. Eissa, A.-G. A. El-Helby, H. A. Mahdy, M. M. Khalifa, H. A. Elnagar, A. B. Mehany, *et al.*, Discovery of new quinazolin-4 (3H)-ones as VEGFR-2 inhibitors: Design, synthesis, and anti-proliferative evaluation, *Bioorg. Chem.*, 2020, **105**, 104380.

40 M. M. Alanazi, H. A. Mahdy, N. A. Alsaif, A. J. Obaidullah, H. M. Alkahtani, A. A. Al-Mehizia, *et al.*, New bis ([1, 2, 4] triazolo)[4, 3-a: 3′, 4′-c] quinoxaline derivatives as VEGFR-2 inhibitors and apoptosis inducers: Design, synthesis, in silico studies, and anticancer evaluation, *Bioorg. Chem.*, 2021, **112**, 104949.

41 N. A. Alsaif, M. S. Taghour, M. M. Alanazi, A. J. Obaidullah, W. A. Alanazi, A. Alasmari, *et al.*, Identification of new [1, 2, 4] triazolo [4, 3-a] quinoxalines as potent VEGFR-2 tyrosine kinase inhibitors: Design, synthesis, anticancer evaluation, and in silico studies, *Bioorg. Med. Chem.*, 2021, **46**, 116384.

42 R. Talaat, W. El-Sayed, H. Agwa, A. Gamal-Eldeen, S. Moawia and M. Zahran, Novel thalidomide analogs: Anti-angiogenic and apoptotic effects on Hep-G2 and MCF-7 cancer cell lines, *Biomed. Aging Pathol.*, 2014, **4**(3), 179–189.

43 T. Inoue, K. Kibata, M. Suzuki, S. Nakamura, R. Motoda and K. Orita, Identification of a vascular endothelial growth factor (VEGF) antagonist, sFlt-1, from a human hematopoietic cell line NALM-16, *FEBS Lett.*, 2000, **469**(1), 14–18.

44 R. M. Talaat, Soluble angiogenesis factors in sera of Egyptian patients with hepatitis C virus infection: correlation with disease severity, *Viral Immunol.*, 2010, **23**(2), 151–157.

45 E. B. Elkaeed, I. H. Eissa, H. Elkady, A. Abdelalim, A. M. Alqaisi, A. A. Alsfouk, *et al.*, A Multistage In Silico Study of Natural Potential Inhibitors Targeting SARS-CoV-2 Main Protease, *Int. J. Mol. Sci.*, 2022, **23**(15), 8407.

46 E. B. Elkaeed, F. S. Youssef, I. H. Eissa, H. Elkady, A. A. Alsfouk, M. L. Ashour, *et al.*, Multi-Step In Silico Discovery of Natural Drugs against COVID-19 Targeting Main Protease, *Int. J. Mol. Sci.*, 2022, **23**(13), 6912.

47 E. B. Elkaeed, R. G. Yousef, H. Elkady, I. M. M. Gobaara, B. A. Alsfouk, D. Z. Husein, *et al.*, Design, Synthesis, Docking, DFT, MD Simulation Studies of a New Nicotinamide-Based Derivative: In Vitro Anticancer and VEGFR-2 Inhibitory Effects, *Molecules*, 2022, **27**(14), 4606.